

1 **Direct probing of Acylperoxy radicals during ozonolysis of  $\alpha$ -pinene: composition,**  
2 **formation mechanism, and contribution to constraints on radical chemistry and the**  
3 **production of highly oxygenated organic molecules**

4 Han Zang<sup>1</sup>, Dandan Huang<sup>2</sup>, Jiali Zhong<sup>3</sup>, Ziyue Li<sup>1</sup>, Chenxi Li<sup>1</sup>, Huayun Xiao<sup>1</sup>, Yue Zhao<sup>1,\*</sup>

5

6 <sup>1</sup>School of Environmental Science and Engineering, Shanghai Jiao Tong University, Shanghai,  
7 200240, China

8 <sup>2</sup>Shanghai Academy of Environmental Sciences, Shanghai 200233, China

9 <sup>3</sup>Division of Environment and Sustainability, Hong Kong University of Science and Technology,  
10 Hong Kong SAR, 999077, China

11

12 \*Correspondence: Yue Zhao (yuezhao20@sjtu.edu.cn)

13

14 **Abstract**

15 Acylperoxy radicals (RO<sub>2</sub>) are key intermediates in atmospheric oxidation of organic compounds  
16 and different from the general alkyl RO<sub>2</sub> radicals in reactivity. However, direct probing of the  
17 molecular identities and chemistry of acyl RO<sub>2</sub> remains quite limited. Here, we report a combined  
18 experimental and kinetic modelling study of the composition and formation mechanisms of acyl  
19 RO<sub>2</sub>, as well as their contributions to the formation of highly oxygenated organic molecules (HOMs)  
20 during ozonolysis of  $\alpha$ -pinene. We find that acyl RO<sub>2</sub> radicals account for 67%, 94%, and 32% of  
21 the highly oxygenated C<sub>7</sub>, C<sub>8</sub>, and C<sub>9</sub> RO<sub>2</sub>, respectively, but only a few percent of C<sub>10</sub> RO<sub>2</sub>. The  
22 formation pathway of acyl RO<sub>2</sub> species depends on their oxygenation level. The highly oxygenated  
23 acyl RO<sub>2</sub> (oxygen atom number  $\geq 6$ ) are mainly formed by the intramolecular aldehydic H-shift (i.e.,  
24 autoxidation) of RO<sub>2</sub>, while the less oxygenated acyl RO<sub>2</sub> (oxygen atom number  $< 6$ ) are basically  
25 derived from the C-C bond cleavage of alkoxy (RO) radicals containing an  $\alpha$ -ketone group or the  
26 intramolecular H-shift of RO containing an aldehyde group. The acyl RO<sub>2</sub>-involved reactions  
27 explain 50-90% of C<sub>7</sub> and C<sub>8</sub> closed-shell HOMs and 14% of C<sub>10</sub> HOMs, respectively. For C<sub>9</sub> HOMs,  
28 this contribution can be up to 30%-60%. In addition, acyl RO<sub>2</sub> contribute to 50%-95% of C<sub>14</sub>-C<sub>18</sub>  
29 HOM dimer formation. Because of the generally fast reaction kinetics of acyl RO<sub>2</sub>, the acyl RO<sub>2</sub> +  
30 alkyl RO<sub>2</sub> reactions seem to outcompete the alkyl RO<sub>2</sub> + alkyl RO<sub>2</sub> pathways, thereby affecting the  
31 fate of alkyl RO<sub>2</sub> and HOM formation. Our study sheds lights on the detailed formation pathways  
32 of the monoterpene-derived acyl RO<sub>2</sub> and their contributions to HOM formation, which will help to  
33 understand the oxidation chemistry of monoterpenes and sources of low-volatility organic  
34 compounds capable of driving particle formation and growth in the atmosphere.

## 35 1. Introduction

36 Monoterpenes ( $C_{10}H_{16}$ ) comprise an important fraction of nonmethane hydrocarbons in the global  
37 atmosphere (Guenther et al. 2012, Sindelarova et al. 2014) and make a significant contribution to  
38 the secondary organic aerosol (SOA) budget (Pye et al. 2010, Iyer et al. 2021). The presence of  
39 double bond and large molecular size of monoterpenes favor their oxidation reactivity towards  $O_3$ ,  
40 hydroxyl (OH), and nitrate ( $NO_3$ ) radicals (Berndt 2022, Roger et al. 2004, Atkinson, Hasegawa  
41 and Aschmann 1990, Kurten et al. 2015, Kristensen et al. 2016, Bianchi et al. 2019), as well as the  
42 formation of low-volatility products and SOA (Molteni et al. 2019, Shen et al. 2022, Bianchi et al.  
43 2019, Zhang et al. 2018, Fry et al. 2014, Fry et al. 2009). The organic peroxy radicals ( $RO_2$ ) in the  
44 gas-phase oxidation of monoterpenes can undergo autoxidation and form a class of highly  
45 oxygenated organic compounds (HOM) (Bianchi et al. 2019, Jokinen et al. 2014, Mentel et al. 2015,  
46 Berndt et al. 2016, Berndt 2022, Zhao, Thornton and Pye 2018, Bell et al. 2021), which are primarily  
47 low- or extremely low-volatility organic compounds (LVOCs and ELVOCs) (Bianchi et al. 2019,  
48 Ehn et al. 2014) and thus play a crucial role in SOA formation and growth.

49 Significant advances have been made in recent years concerning the monoterpene  $RO_2$  autoxidation  
50 and its contribution to HOM formation (Zhao et al. 2018, Shen et al. 2022, Ehn et al. 2014, Berndt  
51 et al. 2016, Xu et al. 2019, Berndt 2022, Lin et al. 2021). It is recognized that a part of monoterpene  
52  $RO_2$  radicals derived from the traditional ozonolysis channel (i.e., isomerization of Criegee  
53 intermediates, CI) and OH addition channel can autoxidize at a rate larger than  $1\text{ s}^{-1}$  and could be  
54 an important contributor to HOM formation (Zhao et al. 2018, Xu et al. 2019, Berndt 2021).  
55 Recently, new reaction channels leading to the  $RO_2$  radicals that can undergo fast autoxidation have  
56 been proposed. A quantum chemical calculation study indicated that an excited CI arising from  $\alpha$ -  
57 pinene ozonolysis could undergo ring-breaking reactions and directly lead to a ring-opened  $RO_2$  due  
58 to the excess energy, which can autoxidize at a rate of  $\sim 1\text{ s}^{-1}$  and rapidly form highly oxidized  $RO_2$   
59 with up to 8 oxygen atoms (Iyer et al. 2021). In addition, the minor hydrogen abstraction channel  
60 by OH radicals has been proposed as a predominant pathway to HOM formation from OH oxidation  
61 of  $\alpha$ -pinene under atmospheric conditions (Shen et al. 2022).

62  $RO_2$  species can be simply divided into alkyl  $RO_2$  and acyl  $RO_2$  ( $RC(O)OO$ ) according to whether  
63 R is an acyl radical. There are significant differences in the reactivity of these two kinds of  $RO_2$ .  
64 Firstly, the rate constant of acyl  $RO_2$  with NO is in general slightly higher than that of alkyl  $RO_2$   
65 (Orlando and Tyndall 2012, Calvert et al. 2008, Atkinson et al. 2007). For example, the reaction  
66 rate constants of acyl  $RO_2$ ,  $CH_3C(O)O_2$ , and alkyl  $RO_2$ ,  $CH_3CH_2O_2$ , with NO have been reported to  
67 be  $20 \times 10^{-12}\text{ cm}^3\text{ molecule}^{-1}\text{ s}^{-1}$  and  $9.2 \times 10^{-12}\text{ cm}^3\text{ molecule}^{-1}\text{ s}^{-1}$ , respectively (Orlando and Tyndall

68 2012, Calvert et al. 2008, Atkinson et al. 2007). Besides, acyl RO<sub>2</sub> can react rapidly with NO<sub>2</sub> and  
69 form thermally unstable peroxyacyl nitrates (RC(O)OONO<sub>2</sub>), which have a lifetime of tens of  
70 minutes at room temperature and of days and even months in winter or in the upper atmosphere with  
71 lower temperatures (Orlando and Tyndall 2012, Atkinson et al. 2007). Although alkyl RO<sub>2</sub> radicals  
72 can also react with NO<sub>2</sub> and form the alkyl peroxy nitrates (ROONO<sub>2</sub>), they are extremely unstable  
73 and will decompose into RO<sub>2</sub> radicals and NO<sub>2</sub> in less than 1s (Orlando and Tyndall 2012, Kirchner  
74 et al. 1997). Lastly, the rate constant of cross-reaction of acyl RO<sub>2</sub> ( $1.5 \pm 0.3 \times 10^{-11} \text{ cm}^3 \text{ molecule}^{-1} \text{ s}^{-1}$ )  
75 is significantly higher than that of alkyl RO<sub>2</sub> ( $2 \times 10^{-17} - 1 \times 10^{-11} \text{ cm}^3 \text{ molecule}^{-1} \text{ s}^{-1}$ ) (Zhao et  
76 al. 2018, Tyndall et al. 2001, Atkinson et al. 2007, Villenave and Lesclaux 1996). As a result, these  
77 two kinds of RO<sub>2</sub> may play different roles in the autoxidation as well as HOM and dimer formation.

78 The quantum calculations revealed that different functional groups in RO<sub>2</sub> would lead to  
79 significantly different intramolecular H-shift rates (Otkjær et al. 2018). The C=O and C=C  
80 substituents lead to resonance stabilized carbon radicals and could enhance the H-shift rate constants  
81 by more than a factor of 400. The fast aldehydic H-shift rate contributes to a series of acyl radicals  
82 (RC(O)) with the radical site at the terminal carbonyl carbon, which further produce the acyl RO<sub>2</sub>  
83 with O<sub>2</sub> addition. Many RO<sub>2</sub> formed in the oxidation of monoterpenes have the aldehyde  
84 functionality, especially for  $\alpha$ -pinene ozonolysis, in which all the primary and many later-generation  
85 RO<sub>2</sub> contain at least one aldehyde group (Berndt et al. 2018, Berndt 2022, Li et al. 2019, Noziere et  
86 al. 2015, Shen et al. 2022). As a result, acyl RO<sub>2</sub> may comprise a considerable fraction of total RO<sub>2</sub>  
87 species and contribute significantly to the formation of low-volatility products and SOA in the  
88 monoterpene oxidation system. A recent study by Zhao et al. (2022) found that the acyl RO<sub>2</sub>-  
89 involved reactions contribute to 50%-80% of oxygenated C<sub>15</sub>-C<sub>20</sub> dimers (O:C  $\geq$  0.4) and 70% of  
90 C<sub>15</sub>-C<sub>19</sub> dimer esters in SOA from  $\alpha$ -pinene ozonolysis. However, currently the direct probing of  
91 the molecular identities and chemistry of monoterpene-derived acyl RO<sub>2</sub> radicals is rather limited.  
92 The role of acyl RO<sub>2</sub> in HOM formation remains to be quantified.

93 In this study, the molecular identities and formation mechanisms of acyl RO<sub>2</sub> radicals, as well as  
94 their contributions to HOM formation in the  $\alpha$ -pinene ozonolysis are investigated. The experiments  
95 were conducted in a flow reactor with different concentrations of NO<sub>2</sub>, which acted as an efficient  
96 scavenger for the acyl RO<sub>2</sub>. The molecular composition and abundance of the gas-phase HOMs  
97 were measured by a chemical ionization-atmospheric pressure interface-time-of-flight mass  
98 spectrometer (CI-APi-TOF) using nitrate as the reagent ions. In addition, kinetic modelling using  
99 the Framework for 0-D Atmospheric Modeling (F0AM v4.1) employing Master Chemical  
100 Mechanisms (MCM v3.3.1) updated with the latest advances of the RO<sub>2</sub> chemistry was performed

101 to gain insights into the reaction kinetics and mechanisms of acyl RO<sub>2</sub> species. We find that acyl  
102 RO<sub>2</sub> account for a major fraction of highly oxygenated C<sub>7</sub> and C<sub>8</sub> RO<sub>2</sub> and play a significant role in  
103 the formation of HOM monomers and dimers with small molecular size. This study will help to  
104 understand the role of acyl RO<sub>2</sub> in the formation of low-volatility species from monoterpene  
105 oxidation and reduce the uncertainties in the future atmospheric modelling of the formation and  
106 impacts of aerosols.

## 107 **2. Method and Materials**

### 108 **2.1 Flow Reactor Experiments.**

109 The  $\alpha$ -pinene ozonolysis experiments were carried out under room temperature (298 K) and dry  
110 conditions (relative humidity < 5%) in a custom-built flow reactor, which has been described in detail  
111 previously (Yao et al. 2019). The  $\alpha$ -pinene vapor was generated by evaporating its pure liquid (99%,  
112 Sigma-Aldrich) into a flow of zero air (10.65 L min<sup>-1</sup>) added to the reactor using an automated  
113 syringe pump (TYD01-01-CE, Baoding Leifu Fluid Technology Co., Ltd.). The initial  
114 concentrations of  $\alpha$ -pinene ranged from 500 ppb to 3 ppm in different experiments. Ozone was  
115 generated by passing a flow of ultra-high-purity (UHP) O<sub>2</sub> (150 mL min<sup>-1</sup>, Shanghai Maytor Special  
116 Gas Co., Ltd.) through a quartz tube housing a pen-ray mercury lamp (UV-S2, UVP Inc.) and its  
117 concentration (45 ppb and 180 ppb under low and high O<sub>3</sub> conditions, respectively) was measured  
118 by an ozone analyzer (Model 49i, Thermo Fisher Scientific, USA). The NO<sub>2</sub>, acting as an acyl RO<sub>2</sub>  
119 scavenger, was derived from its standard cylinder gas (15.6 ppm, Shanghai Weichuang Standard  
120 Gas Co., Ltd.) and its initial concentration ranged from 0 to 30 ppb. To validate the formation  
121 mechanisms of acyl RO<sub>2</sub>, selected experiments with the addition of NO or cyclohexane were also  
122 conducted. NO was derived by its standard cylinder gas (9.8 ppm, Shanghai Weichuang Standard  
123 Gas Co., Ltd.) and its initial concentration also ranged from 0 to 30 ppb. The gas-phase cyclohexane  
124 (~ 500 ppm), acting as an OH scavenger, was generated by bubbling a gentle flow of UHP N<sub>2</sub>  
125 through liquid cyclohexane (LC-MS grade, CNW). The total air flow in the flow reactor was 10.8 L  
126 min<sup>-1</sup> and the residence time was 25 seconds. The relatively low O<sub>3</sub> concentration and short reaction  
127 time in the flow reactor avoid significant production of NO<sub>3</sub> radicals from NO<sub>2</sub> and O<sub>3</sub> and make  
128 the NO<sub>3</sub> oxidation contribute only 0.3%-1.2% of the total  $\alpha$ -pinene oxidation in our experiments.  
129 Therefore, the NO<sub>3</sub> chemistry could be neglected in this study. A summary of the experimental  
130 conditions is given in Tables S1 and S2 in the Supplement.

131 The gas-phase RO<sub>2</sub> radicals and closed-shell products were measured by a nitrate-based CI-API-  
132 TOF mass spectrometer (abbreviated as nitrate-CIMS; Aerodyne Research, Inc.), and a long time-  
133 of-flight mass spectrometer with a mass resolution of ~10000 Th/Th was used here. The mass

134 calibration error is below 1.8 ppm. The sheath flow, including a 2 mL min<sup>-1</sup> UHP N<sub>2</sub> flow containing  
 135 nitric acid (HNO<sub>3</sub>) and 22.4 L min<sup>-1</sup> zero air was guided through a PhotoIonizer X-ray (Model L9491,  
 136 Hamamatsu, Japan) to generate nitrate reagent ions. The total sample flow rate was 9 L min<sup>-1</sup> during  
 137 the experiments. ~~The instrument was calibrated with a sulfuric acid (H<sub>2</sub>SO<sub>4</sub>) calibration factor and~~  
 138 ~~a mass dependent transmission efficiency.~~ The mass spectra within the m/z range of 50 to 700 were  
 139 analyzed using the tofTools package developed by Junninen et al. (2010) based on Matlab. ~~After~~  
 140 ~~getting the signals of the gas phase oxygenated organic molecules (OOMs), their concentration can~~  
 141 ~~be calculated as follows~~ (Jokinen et al. 2012, Bianchi et al. 2019):

$$142 \quad [OOM] = C \times \frac{I_{OOM}}{I_{NO_3^-} + I_{HNO_3NO_3^-} + I_{HNO_3HNO_3NO_3^-}} \times \frac{1}{T_i} \quad (1)$$

143 ~~C is the calibration factor of H<sub>2</sub>SO<sub>4</sub>, with a value of 4.06 × 10<sup>9</sup> molecule cm<sup>-3</sup> in this study; I<sub>X</sub> is the~~  
 144 ~~detected signal of X in the unit of counts per second (cps) and most OOMs were detected as adducts~~  
 145 ~~with NO<sub>3</sub><sup>-</sup>; T<sub>i</sub> is the mass dependent transmission efficiency of the instrument determined using the~~  
 146 ~~following equation by adding propanoic acid, pentanoic acid and heptanoic acid vapors to deplete~~  
 147 ~~NO<sub>3</sub><sup>-</sup> (Figure S1):~~

$$148 \quad T_i = 0.56 + 7.2 \times 10^4 / ((m/z - 498.84)^2 + 3.46 \times 10^4) \quad (2)$$

149 To clarify whether there is SOA formation in the experiments, a scanning mobility particle sizer  
 150 (SMPS, TSI), which consists of an electrostatic classifier (model 3080), a long or nano differential  
 151 mobility analyzer (model 3081 and 3085 for different particle sizes), and a condensation particle  
 152 counter (model 3087), was used to monitor the formation of SOA particles. Except in Exp 31 where  
 153 the reacted α-pinene reached 36.8 ppb and there was low SOA formation with particle mass  
 154 concentrations of 5.0×10<sup>-4</sup>-5.7×10<sup>-3</sup> μg m<sup>-3</sup> and number concentrations of 63-395 cm<sup>-3</sup>, no particle  
 155 formation was observed by SMPS. Therefore, the RO<sub>2</sub> radicals and closed-shell products would be  
 156 primarily distributed in the gas-phase, with their fates negligibly influenced by the low SOA  
 157 formation under these experimental conditions.

## 158 2.2 Kinetic Model Simulations.

159 Model simulations of RO<sub>2</sub> and HOM formation in selected experiments were performed to constrain  
 160 the reaction kinetics and mechanisms of acyl RO<sub>2</sub> using FOAM v4.1 (Wolfe et al. 2016), which  
 161 employs MCM v3.3.1 (Jenkin, Young and Rickard 2015) updated with the chemistry of RO<sub>2</sub>  
 162 autoxidation and cross-reactions forming HOM monomers and dimers. Newly added species and  
 163 reactions to MCM v3.3.1 followed the work by Zhao et al. (2018) and Wang et al. (2021).  
 164 Considering that the default MCM v3.3.1 does not include highly oxygenated acyl RO<sub>2</sub>, we added

165 the possible formation pathways of the potential acyl RO<sub>2</sub> measured in this study to the model based  
166 on the mechanisms proposed by Zhao et al. (2022).

167 The formation and reaction branching ratios of the two  $\alpha$ -pinene-derived CIs are updated in the  
168 model according to the recent studies (Table S3) (Wang et al. 2021, Berndt 2022, Iyer et al. 2021,  
169 Clafin et al. 2018). The formation of a ring-opened C<sub>10</sub>H<sub>15</sub>O<sub>4</sub>-RO<sub>2</sub> species (C10H15O4RBRO2 in  
170 Table S3) from  $\alpha$ -pinene ozonolysis proposed by a recent study (Iyer et al. 2021), as well as its  
171 subsequent autoxidation and bimolecular reactions, is included in the model. The autoxidation rate  
172 constant of the ring-opened C<sub>10</sub>H<sub>15</sub>O<sub>4</sub>-RO<sub>2</sub> is 1 s<sup>-1</sup>, and a lower limit of its molar yield (30%) was  
173 used according to the recent studies (Wang et al. 2021, Meder et al. 2023) and our results (see details  
174 in Section 3.3). We also added the hydrogen abstraction channel of  $\alpha$ -pinene oxidation by OH  
175 radicals according to a recent study (Shen et al. 2022). The branching ratio of this channel was set  
176 to 9%, with the rest 91% being the traditional OH addition pathways. The detailed reaction pathways  
177 and rate constants of RO<sub>2</sub> species in this channel followed the work by Shen et al. (2022), except  
178 for RO<sub>2</sub> cross-reactions, the rates of which were not reported in that study. As the primary RO<sub>2</sub>  
179 radicals (C<sub>10</sub>H<sub>15</sub>O<sub>2</sub>-RO<sub>2</sub>) formed via the hydrogen abstraction by OH radical are least-oxidized with  
180 only 2 oxygen atoms, their cross-reaction rate could be relatively low (Atkinson et al. 2007, Orlando  
181 and Tyndall 2012). In the model, this rate constant was set to 1 × 10<sup>-13</sup> cm<sup>3</sup> molecule<sup>-1</sup> s<sup>-1</sup>. For other  
182 alkyl RO<sub>2</sub> radicals (including HOM-RO<sub>2</sub>), their cross-reaction rate constant is assumed to be 1 × 10<sup>-</sup>  
183 <sup>12</sup> cm<sup>3</sup> molecule<sup>-1</sup> s<sup>-1</sup> according to Zhao et al. (2018). The dimer formation rates for these alkyl RO<sub>2</sub>  
184 are same as their cross-reaction rates.

185 In flow reactor experiments, the equilibrium formation of ROONO<sub>2</sub> would lead to the consumption  
186 of alkyl RO<sub>2</sub> radicals. To account for the influence of this process on the RO<sub>2</sub> budget and HOM  
187 formation, we included the reaction of RO<sub>2</sub> + NO<sub>2</sub> ⇌ ROONO<sub>2</sub> in the model, with forward and  
188 reverse reaction rate constants of 7.5 × 10<sup>-12</sup> cm<sup>3</sup> molecule<sup>-1</sup> s<sup>-1</sup> and 5 s<sup>-1</sup>, respectively (Orlando and  
189 Tyndall 2012). To simplify the parameterization, the forward and reverse reaction rate constants of  
190 newly added highly oxygenated acyl RO<sub>2</sub> with NO<sub>2</sub> are the same as default values in MCM v3.3.1.  
191 Besides, the cross-reaction rate constants of acyl RO<sub>2</sub> (including acyl RO<sub>2</sub> + acyl RO<sub>2</sub> and acyl RO<sub>2</sub>  
192 + alkyl RO<sub>2</sub>) forming monomers or dimers were both set to 1 × 10<sup>-11</sup> cm<sup>3</sup> molecule<sup>-1</sup> s<sup>-1</sup> (Orlando  
193 and Tyndall 2012). Considering that there are large uncertainties in the dimer formation rate of RO<sub>2</sub>,  
194 a sensitivity analysis was conducted to evaluate its influence on acyl RO<sub>2</sub>-involved HOM formation  
195 by varying the rate constant from 1 × 10<sup>-13</sup> cm<sup>3</sup> molecule<sup>-1</sup> s<sup>-1</sup> to 1 × 10<sup>-12</sup> cm<sup>3</sup> molecule<sup>-1</sup> s<sup>-1</sup> for alkyl  
196 RO<sub>2</sub> and 1 × 10<sup>-12</sup> cm<sup>3</sup> molecule<sup>-1</sup> s<sup>-1</sup> to 1 × 10<sup>-11</sup> cm<sup>3</sup> molecule<sup>-1</sup> s<sup>-1</sup> for acyl RO<sub>2</sub>. The results show  
197 that changes in dimer formation rate constants within the above ranges have no significant influence

198 on the contribution of acyl RO<sub>2</sub> to HOM formation (Figure S2S1).

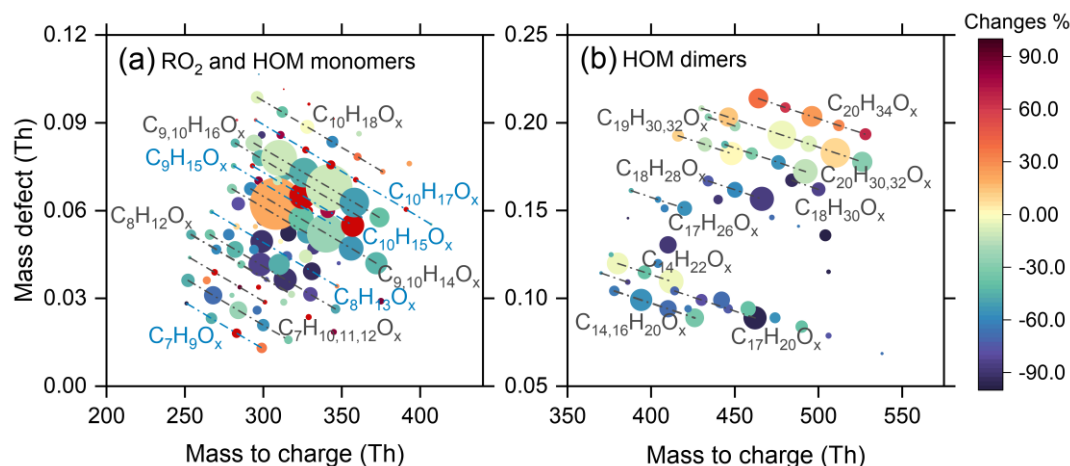
199 The wall losses of OH, HO<sub>2</sub>, and RO<sub>2</sub> radicals, as well as closed-shell HOM monomers and dimers  
200 in the flow reactor were considered using the KPS method proposed by Knopf et al. (2015) in the  
201 model (Table S4), with an assumption of irreversible uptake of these species on the reactor wall. It  
202 is found that the wall loss of OH, HO<sub>2</sub>, and RO<sub>2</sub> radicals accounts for 0.08-0.14%, 4.7-9.1%, and 7.3-  
203 25.5% of their total production, respectively, with lower values under higher reacted  $\alpha$ -pinene  
204 concentration conditions. Therefore, the wall loss process would not significantly influence  $\alpha$ -  
205 pinene oxidation and RO<sub>2</sub> chemistry. The wall losses of closed-shell HOM monomers and dimers  
206 account for 18.4-34.7% and 14.2-33.1% of their total production, respectively. It should be noted  
207 that the wall losses of typical RO<sub>2</sub> and HOMs have negligible impact on their responses to the  
208 addition of NO<sub>2</sub> (Figure S3S2). In addition, with the consideration of the wall loss effects, the effect  
209 and contribution of acyl RO<sub>2</sub> to the HOM formation only changed a little (0.02-0.5%). Therefore,  
210 the wall losses of RO<sub>2</sub> and HOMs in the flow reactor would not affect the interpretation of the results  
211 in this study.

### 212 3. Results and Discussion

#### 213 3.1 Molecular composition of acyl RO<sub>2</sub> from $\alpha$ -pinene ozonolysis

214 The overall formation characteristics of gas-phase RO<sub>2</sub>, closed-shell monomers, and dimers with  
215 the addition of NO<sub>2</sub> (30 ppb) is shown in Figure 1 (Exps 8 and 14, Table S1). Since nitrate-CIMS is  
216 only highly sensitive to the highly oxygenated species, we only discuss the production of HOMs  
217 with oxygen atoms above 6 here. As for RO<sub>2</sub> and closed-shell monomers (Figure 1a), the  
218 ~~concentrations-signals~~ of C<sub>7</sub> and C<sub>8</sub> species decrease by more than 50% with the addition of NO<sub>2</sub>,  
219 while for C<sub>9</sub> and C<sub>10</sub> species, their decreases are relatively small (within 40%). In addition, we note  
220 that there is an unexpected increase in some C<sub>9</sub> and C<sub>10</sub> RO<sub>2</sub>, and the possible reason will be  
221 discussed in detail in Section 3.3.





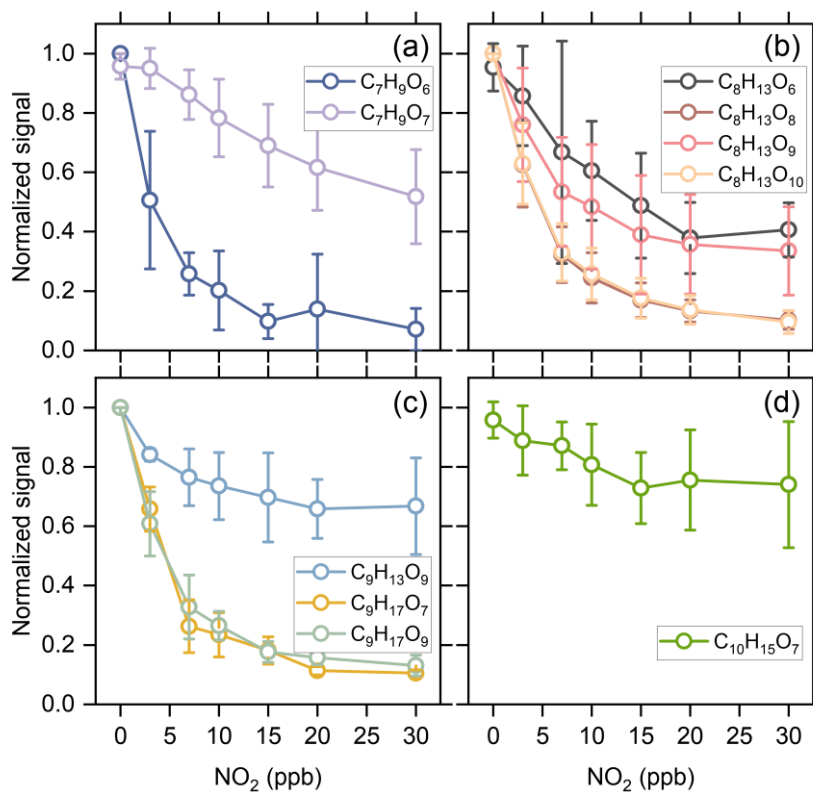
222

223 Figure 1 Mass defect plots of (a) RO<sub>2</sub>, HOM monomers, and (b) HOM dimers formed from  
 224 ozonolysis of  $\alpha$ -pinene in the presence of NO<sub>2</sub> measured using nitrate-CIMS (Exps 8, 14). The  
 225 circles are colored by the relative changes in concentration-signal of RO<sub>2</sub>, monomers and dimers  
 226 due to the addition of NO<sub>2</sub> (30 ppb). The area of circles is linearly scaled with the cube root of the  
 227 concentration-signal of HOMs formed in the absence of NO<sub>2</sub>. The blue lines represent RO<sub>2</sub> radicals.

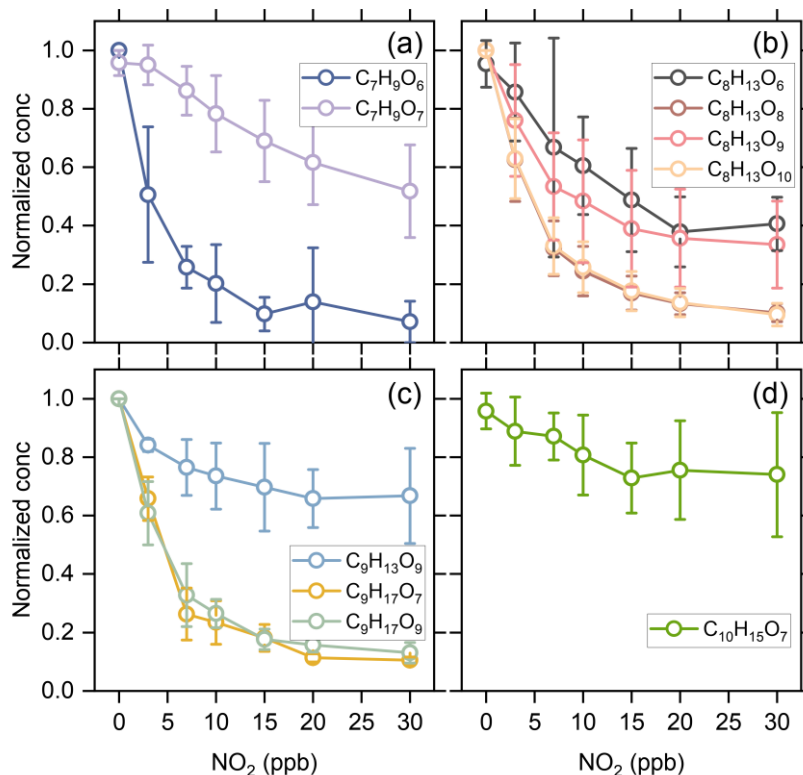
228 NO<sub>2</sub> could react rapidly with acyl RO<sub>2</sub> radicals to form RC(O)OONO<sub>2</sub>, which has a higher thermal-  
 229 stability compared to ROONO<sub>2</sub> and can serve as a sink for acyl RO<sub>2</sub> on our experimental timescales.  
 230 Therefore, a significant decrease in C<sub>7</sub> and C<sub>8</sub> RO<sub>2</sub> and HOMs upon the addition of NO<sub>2</sub> indicates  
 231 that a major fraction of C<sub>7</sub> and C<sub>8</sub> RO<sub>2</sub> are acyl RO<sub>2</sub>. In contrast, the slight decrease in C<sub>9</sub> and C<sub>10</sub>  
 232 HOM monomers shows that the contribution of acyl RO<sub>2</sub> to C<sub>9</sub> and C<sub>10</sub> RO<sub>2</sub> is relatively small.  
 233 However, some of the C<sub>10</sub> monomers showed a slight increase with the addition of NO<sub>2</sub>, especially  
 234 for C<sub>10</sub>H<sub>18</sub>O<sub>x</sub>-HOMs. The addition of NO<sub>2</sub> plays a twofold role in dimer formation from  $\alpha$ -pinene  
 235 ozonolysis (Figure 1b). There is a significant inhibiting effect on C<sub>14</sub>-C<sub>18</sub> dimers, which is due to  
 236 the large contribution of acyl RO<sub>2</sub> to the total C<sub>7</sub> and C<sub>8</sub> RO<sub>2</sub> that generate such dimers. However,  
 237 C<sub>19</sub> and C<sub>20</sub> dimers only show a slight decrease with the addition of NO<sub>2</sub>, and some of them are even  
 238 enhanced. In particular, the enhancement in C<sub>20</sub>H<sub>34</sub>O<sub>x</sub> is most significant, reaching 30%.

239 Kinetic model simulations show that the concentration of alkyl RO<sub>2</sub> decreases by 1-20% with the  
 240 addition of 30 ppb NO<sub>2</sub> under different reacted  $\alpha$ -pinene conditions (Exps 1-28). Considering that  
 241 the acyl RO<sub>2</sub> could be rapidly consumed by NO<sub>2</sub>, if the concentration-signal reduction of a RO<sub>2</sub>  
 242 species significantly exceeds 20% with 30 ppb NO<sub>2</sub> addition, we presume it has significant  
 243 contribution from acyl RO<sub>2</sub>. As a result, a total of 10 acyl RO<sub>2</sub> were identified according to the  
 244 changes of RO<sub>2</sub> concentration-signal as a function of initial NO<sub>2</sub> concentration, which include  
 245 C<sub>7</sub>H<sub>9</sub>O<sub>6</sub>, C<sub>7</sub>H<sub>9</sub>O<sub>7</sub>, C<sub>8</sub>H<sub>13</sub>O<sub>6</sub>, C<sub>8</sub>H<sub>13</sub>O<sub>8</sub>, C<sub>8</sub>H<sub>13</sub>O<sub>9</sub>, C<sub>8</sub>H<sub>13</sub>O<sub>10</sub>, C<sub>9</sub>H<sub>13</sub>O<sub>9</sub>, C<sub>9</sub>H<sub>17</sub>O<sub>7</sub>, C<sub>9</sub>H<sub>17</sub>O<sub>9</sub>, and  
 246 C<sub>10</sub>H<sub>15</sub>O<sub>7</sub>. Figure 2 shows the averaged normalized acyl RO<sub>2</sub> concentrations-signals measured as a

247 function of the added  $\text{NO}_2$  concentration under different experimental conditions (Exps 1-28).  
 248 Similarly, since nitrate-CIMS is only highly sensitive to products with high oxygen content, we only  
 249 observed acyl  $\text{RO}_2$  with oxygen atoms above 6. Consistent with the significant decrease in  $\text{C}_7$  and  
 250  $\text{C}_8$  species with the addition of  $\text{NO}_2$  in Figure 1a,  $\text{C}_7$  and  $\text{C}_8$  acyl  $\text{RO}_2$  decrease by more than 50%  
 251 with the increase of  $\text{NO}_2$  concentration (Figures 2a, b). For  $\text{C}_9$  acyl  $\text{RO}_2$ , the  $\text{C}_9\text{H}_{17}\text{O}_7\text{-RO}_2$  and  
 252  $\text{C}_9\text{H}_{17}\text{O}_9\text{-RO}_2$  also decrease dramatically with increasing  $\text{NO}_2$ , and the decrease in  $\text{C}_9\text{H}_{13}\text{O}_9\text{-RO}_2$  is  
 253 relatively smaller (Figure 2c). In addition,  $\text{C}_{10}\text{H}_{15}\text{O}_7\text{-RO}_2$  also shows a small decrease (Figure 2d),  
 254 with a reduction of only 30% at 30 ppb  $\text{NO}_2$ . The relatively small reduction in the abundance  
 255 of some of these  $\text{RO}_2$  radicals indicates the presence of alkyl  $\text{RO}_2$  radicals with the same chemical  
 256 formulas. Along with the marked reduction in acyl  $\text{RO}_2$  signals, the production of highly oxygenated  
 257  $\text{RC(O)OONO}_2$  species such as  $\text{C}_9\text{H}_{13}\text{O}_9\text{NO}_2$ ,  $\text{C}_9\text{H}_{17}\text{O}_7\text{NO}_2$ , and  $\text{C}_{10}\text{H}_{15}\text{O}_7\text{NO}_2$  with the addition of  
 258  $\text{NO}_2$  were observed (see the spectra in Figure S3). However, we note that although some  
 259  $\text{RC(O)OONO}_2$  such as  $\text{C}_8\text{H}_{13}\text{O}_6\text{NO}_2$  and  $\text{C}_8\text{H}_{13}\text{O}_8\text{NO}_2$  are expected to be formed with  $\text{NO}_2$  addition,  
 260 they could not be unambiguously detected by nitrate-CIMS due to the overlapping of their peaks  
 261 with strong alkyl  $\text{RO}_2$  peaks ( $\text{C}_9\text{H}_{15}\text{O}_8\text{-RO}_2$  and  $\text{C}_9\text{H}_{15}\text{O}_{10}\text{-RO}_2$ ) in this study.



264



265

266 Figure 2 Averaged normalized concentration-signal of the measured acyl RO<sub>2</sub> as a function of the  
 267 added NO<sub>2</sub> concentration under different experimental conditions (Exps 1-28).

268 Figure 3 shows the contribution of acyl and alkyl RO<sub>2</sub> to the highly oxidized C<sub>7</sub>-C<sub>10</sub> RO<sub>2</sub>. Acyl RO<sub>2</sub>  
 269 contribute 67.266.9%, 94.3% and 31.931.7% to the total C<sub>7</sub>, C<sub>8</sub>, and C<sub>9</sub> RO<sub>2</sub> concentrationssignals,  
 270 respectively. By contrast, the only C<sub>10</sub> acyl RO<sub>2</sub> measured in this study is C<sub>10</sub>H<sub>15</sub>O<sub>7</sub>, which  
 271 contributes to only 0.50.4% of the total C<sub>10</sub> RO<sub>2</sub>. It should be note that there might be other C<sub>10</sub> acyl  
 272 RO<sub>2</sub> that were not observed due to the interferences from the alkyl RO<sub>2</sub> with the same chemical  
 273 formulas, which respond differently to the addition of NO<sub>2</sub> than acyl RO<sub>2</sub> do (see details in the  
 274 following discussion). Considering that some RO<sub>2</sub> formulas such as C<sub>10</sub>H<sub>15</sub>O<sub>7</sub> may have  
 275 contributions from both acyl RO<sub>2</sub> and alkyl RO<sub>2</sub>, we assumed the decrease of RO<sub>2</sub> concentration  
 276 signal with the addition of NO<sub>2</sub> as the concentration-signal of acyl RO<sub>2</sub>. Besides, it is obvious that  
 277 the normalized concentration-signal basically decreases to the lowest value when the initial NO<sub>2</sub>  
 278 concentration reaches 10 ppb (Figure 2), indicating that most of the acyl RO<sub>2</sub> are depleted at this  
 279 NO<sub>2</sub> concentration. In addition, the decreasing extents of some acyl RO<sub>2</sub> are different for different  
 280 reacted  $\alpha$ -pinene concentrations, with lower decreasing extent for higher reacted  $\alpha$ -pinene  
 281 concentrations (Figure S4S54). This difference might be due to the promoted cross-reactions of acyl  
 282 RO<sub>2</sub> as well as their precursor RO<sub>2</sub> at higher  $\alpha$ -pinene concentrations, which are competitive with  
 283 the reactions leading to acyl RO<sub>2</sub> formation as well as the acyl RO<sub>2</sub> + NO<sub>2</sub> reactions.

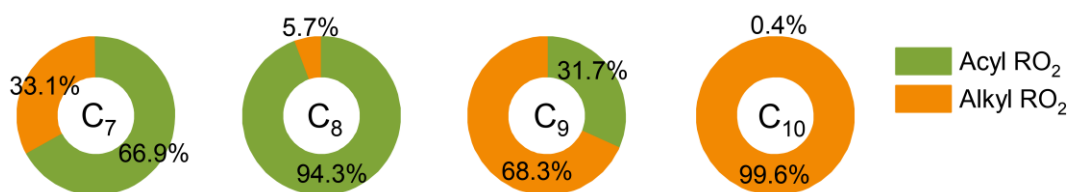


Figure 3 Contributions of acyl and alkyl RO<sub>2</sub> to the highly oxygenated C<sub>7</sub>-C<sub>10</sub> RO<sub>2</sub> measured by nitrate-CIMS.

In addition to the changes of acyl RO<sub>2</sub> [concentration-signal](#), we also show the changes of normalized alkyl RO<sub>2</sub> [concentration-signal](#) with the increasing initial NO<sub>2</sub> concentration in Figure [S5S65](#). Although ROONO<sub>2</sub> formed by the reaction of alkyl RO<sub>2</sub> with NO<sub>2</sub> is thermally unstable and would decompose quickly to release RO<sub>2</sub>, it would still reach a formation/decomposition equilibrium in the system, thus consuming a small amount of alkyl RO<sub>2</sub>. However, it can be seen from Figure [S5S65](#) that during 25 s of reaction in the flow reactor, a large part of alkyl RO<sub>2</sub> has an increasing trend with the increase of NO<sub>2</sub> concentration. We speculate that a portion of ROONO<sub>2</sub> could decompose back to RO<sub>2</sub> and NO<sub>2</sub> in the nitrate-CI inlet where the sample gases were diluted instantly and the equilibrium of ROONO<sub>2</sub> was disturbed, resulting in the release of a large amount of RO<sub>2</sub>.

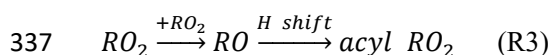
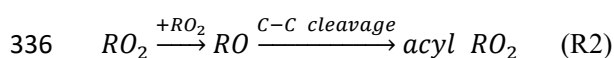
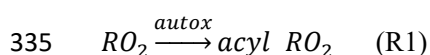
To verify our speculation, the decomposition of ROONO<sub>2</sub> in the CI inlet was simulated based on the dilution ratio (1:3.5) and residence time (200 ms) in the inlet. As shown in Figure [S6S76](#), more than 40% of ROONO<sub>2</sub> decompose back to RO<sub>2</sub> and NO<sub>2</sub> in the CI inlet, which would inevitably lead to an increase in RO<sub>2</sub> concentration. As the C<sub>10</sub>H<sub>15</sub>O<sub>8</sub>NO<sub>2</sub> has a significant contribution from the relative stable RC(O)OONO<sub>2</sub> arising from the ring-opened acyl C<sub>10</sub>H<sub>15</sub>O<sub>8</sub>-RO<sub>2</sub> reported by Iyer et al. (2021), its decomposition is relatively small (~21%). It should be noted that the RO<sub>2</sub> measured here is only a part of total RO<sub>2</sub> and that a large amount of RO<sub>2</sub> has already reacted to form closed-shell products as well as ROONO<sub>2</sub> in the flow reactor. Taking Exp 14 as an example (30 ppb NO<sub>2</sub>), the simulated concentrations of RO<sub>2</sub> and ROONO<sub>2</sub> are 1.3 ppb and 1.9 ppb, which approximately accounts for 27.1% and 39.6% of the total production of RO<sub>2</sub>, respectively. Therefore, the decomposition of ROONO<sub>2</sub> could indeed result in an increase in the RO<sub>2</sub> [concentration-signal](#). It should also be pointed out that because of the very short residence time in the CI inlet, such an increase in the RO<sub>2</sub> concentration would not significantly impact HOM formation.

To confirm the reliability of our results, we examined the changes in the [concentration-signals](#) of RO<sub>2</sub> and closed-shell products as a function of reacted  $\alpha$ -pinene in the absence of NO<sub>2</sub> (Section S1 and Figure [S7S78](#)), and the results are consistent with previous studies (Zhao et al. 2018). In addition, we repeated Exps 15-21 on another nitrate-CIMS and a similar increase in alkyl RO<sub>2</sub> signals with the addition of NO<sub>2</sub> was observed on that instrument (Figure [S8S989](#)).

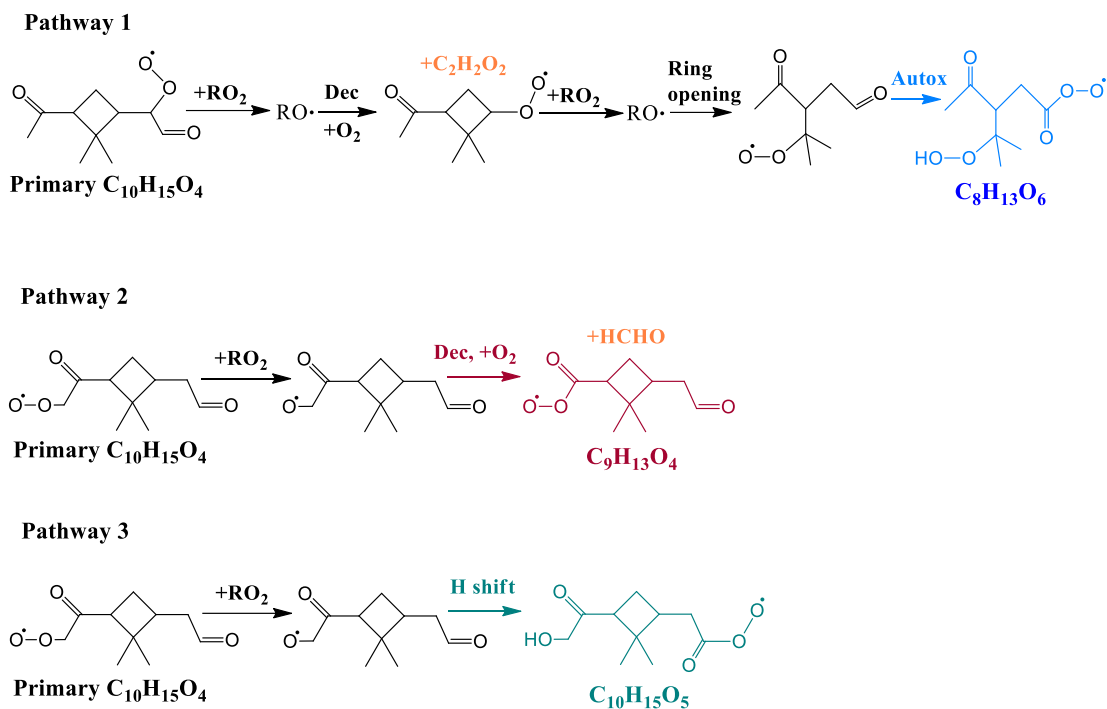
### 315 3.2 Formation mechanisms of acyl RO<sub>2</sub> during $\alpha$ -pinene ozonolysis

316 It has been recently suggested that there are three main pathways that directly lead to the formation  
317 of monoterpene-derived acyl RO<sub>2</sub> (Zhao et al. 2022) (Shen et al. 2022): (i) the autoxidation of RO<sub>2</sub>  
318 containing aldehyde groups (Reaction R1), (ii) the cleavage of C-C bond of RO containing an  $\alpha$ -  
319 ketone group (Reaction R2), and (iii) the intramolecular H-shift of RO containing an aldehyde group  
320 (Reaction R3). In addition, the secondary OH oxidation of aldehyde products can also produce acyl  
321 RO<sub>2</sub> radicals. However, in the present study, the secondary OH oxidation is expected to be  
322 insignificant due to an excess of  $\alpha$ -pinene compared to O<sub>3</sub>. Indeed, kinetic model simulations  
323 incorporating the secondary OH chemistry show that the contribution of secondary OH oxidation to  
324 acyl RO<sub>2</sub> formation is negligible even under high O<sub>3</sub> conditions (see details in Section S2 and Figure  
325 S910).

326 Here, we further investigated the formation mechanisms of acyl RO<sub>2</sub>. Figure 4 shows the reaction  
327 schemes leading to the formation of example acyl RO<sub>2</sub> radicals. The detailed formation mechanisms  
328 of acyl RO<sub>2</sub> measured in this study are shown in Figure S9S101. The formation of acyl RO<sub>2</sub>,  
329 especially those having the small molecular size (C<sub>7</sub>-C<sub>9</sub>), requires the production and subsequent  
330 decomposition (or ring-opening process) of RO radicals. Take C<sub>8</sub>H<sub>13</sub>O<sub>6</sub>-RO<sub>2</sub> as an example (Figure  
331 4), two steps of RO formation and decomposition following the primary C<sub>10</sub>H<sub>15</sub>O<sub>4</sub>-RO<sub>2</sub> lead to the  
332 ring-opened C<sub>8</sub>H<sub>13</sub>O<sub>4</sub>-RO<sub>2</sub> that can undergo rapid aldehydic H-shift to form the acyl RO<sub>2</sub>. While for  
333 C<sub>8</sub>H<sub>13</sub>O<sub>9</sub>-RO<sub>2</sub>, it directly comes from the aldehydic H-shift of C<sub>8</sub>H<sub>13</sub>O<sub>7</sub>-RO followed by the O<sub>2</sub>  
334 addition (Figure S9S1101).

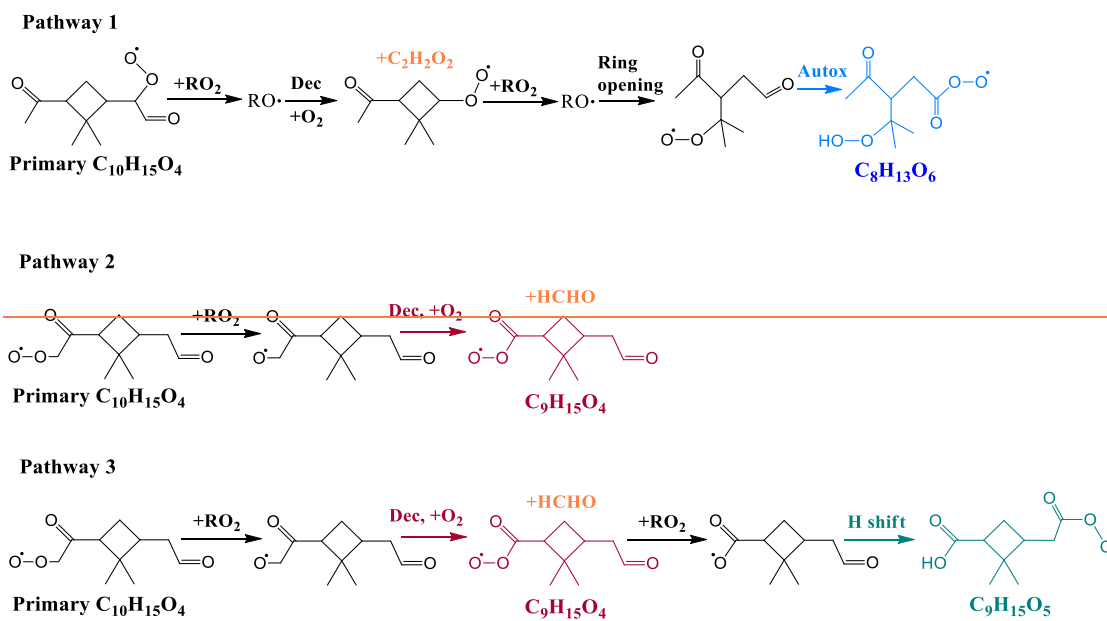


338



339

340 Figure 4 Three different formation pathways of acyl  $RO_2$  during ozonolysis of  $\alpha$ -pinene. The acyl  
 341  $RO_2$ ,  $C_9H_{13}O_4$ - $C_9H_{13}O_4$  and  $C_9H_{15}O_5$ - $C_{10}H_{15}O_5$ , formed via pathways 2 and 3, respectively, were not  
 342 detected by nitrate-CIMS in this study due to their relatively low oxygenation level.

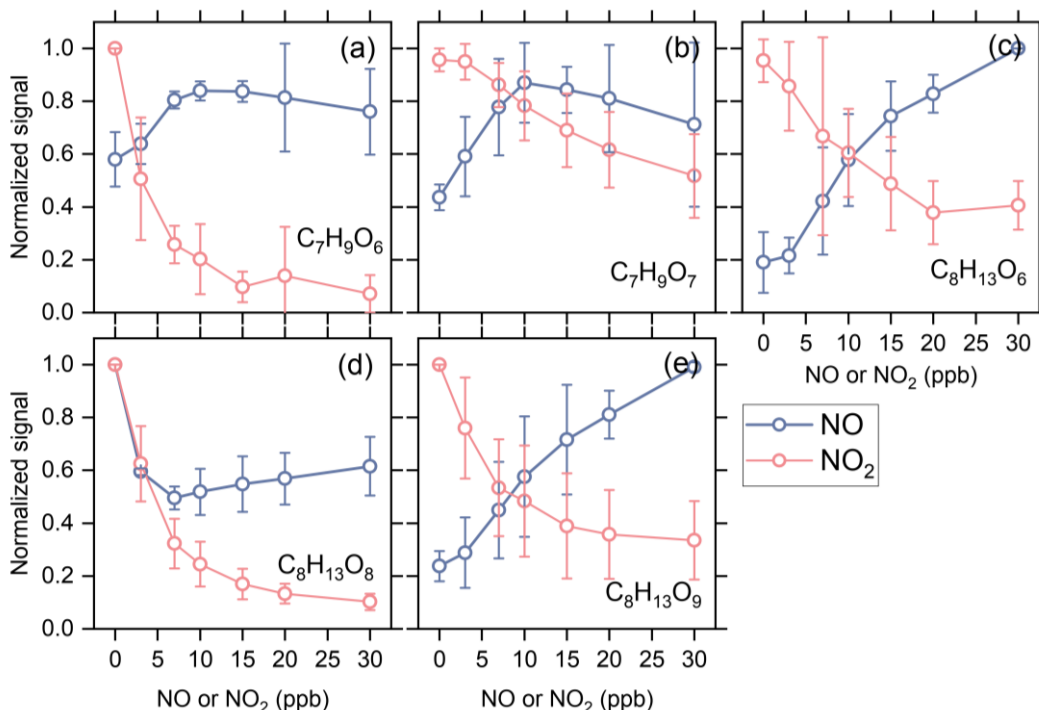


343

344 Figure 4 Three different formation pathways of acyl  $RO_2$  during ozonolysis of  $\alpha$ -pinene. The acyl  
 345  $RO_2$ ,  $C_9H_{15}O_4$ - $C_9H_{13}O_4$  and  $C_9H_{15}O_5$ - $C_{10}H_{15}O_5$ , formed via pathways 2 and 3, respectively, were not  
 346 detected by nitrate-CIMS in this study due to their relatively low oxygenation level.

347 To verify the formation mechanisms of acyl  $RO_2$ , we added NO in some experiments (Exps 33-56)

348 to see how acyl RO<sub>2</sub> respond to the increasing NO concentration. As shown in Figure 5, the changes  
 349 of C<sub>7</sub> and C<sub>8</sub> acyl RO<sub>2</sub> show opposite trend with the increasing NO and NO<sub>2</sub> concentration, except  
 350 for C<sub>8</sub>H<sub>13</sub>O<sub>8</sub>-RO<sub>2</sub>. NO can react with RO<sub>2</sub> to form RO radicals and promote the formation of RO<sub>2</sub>  
 351 that requires the involvement of RO radicals in their formation. In addition to C<sub>8</sub>H<sub>13</sub>O<sub>6</sub>-RO<sub>2</sub>  
 352 discussed above, the formation of C<sub>7</sub>H<sub>9</sub>O<sub>7</sub>-RO<sub>2</sub> and C<sub>8</sub>H<sub>13</sub>O<sub>9</sub>-RO<sub>2</sub> needs 2 and 4 steps of the RO  
 353 formation following C<sub>10</sub>H<sub>15</sub>O<sub>4</sub>-RO<sub>2</sub> (Figure S9S1+04), respectively. Therefore, the increase of RO  
 354 concentration due to the addition of NO would promote the production of these acyl RO<sub>2</sub>. These  
 355 results prove that the RO radicals indeed play an important role in the acyl RO<sub>2</sub> formation. While  
 356 for C<sub>8</sub>H<sub>13</sub>O<sub>8</sub>-RO<sub>2</sub>, its concentration-signal decreases substantially with the addition of NO up to 3  
 357 ppb, similar to the trend observed with the addition of NO<sub>2</sub>. After reaching the minimum at 7 ppb  
 358 NO, the concentration-signal of C<sub>8</sub>H<sub>13</sub>O<sub>8</sub>-RO<sub>2</sub> tends to increase with the further increase of NO  
 359 concentration. Given that C<sub>8</sub>H<sub>13</sub>O<sub>8</sub>-RO<sub>2</sub> is likely to directly come from the autoxidation of C<sub>8</sub>H<sub>13</sub>O<sub>6</sub>  
 360 acyl RO<sub>2</sub> (see Figure S9S1+04), the rapid consumption of C<sub>8</sub>H<sub>13</sub>O<sub>6</sub>-RO<sub>2</sub> by NO and NO<sub>2</sub> (formed  
 361 by O<sub>3</sub> oxidation of NO) may outcompete its autoxidation process, thus leading to a decrease in  
 362 C<sub>8</sub>H<sub>13</sub>O<sub>8</sub>-RO<sub>2</sub> concentrationsignal. Besides, it can be seen that the increasing extent in C<sub>8</sub>H<sub>13</sub>O<sub>6</sub>-  
 363 RO<sub>2</sub> is also relatively small before the NO concentration reaches 3 ppb (Figure 5c), indicating that  
 364 the promotion effect of NO on C<sub>8</sub>H<sub>13</sub>O<sub>6</sub>-RO<sub>2</sub> formation is not that strong at this concentration.



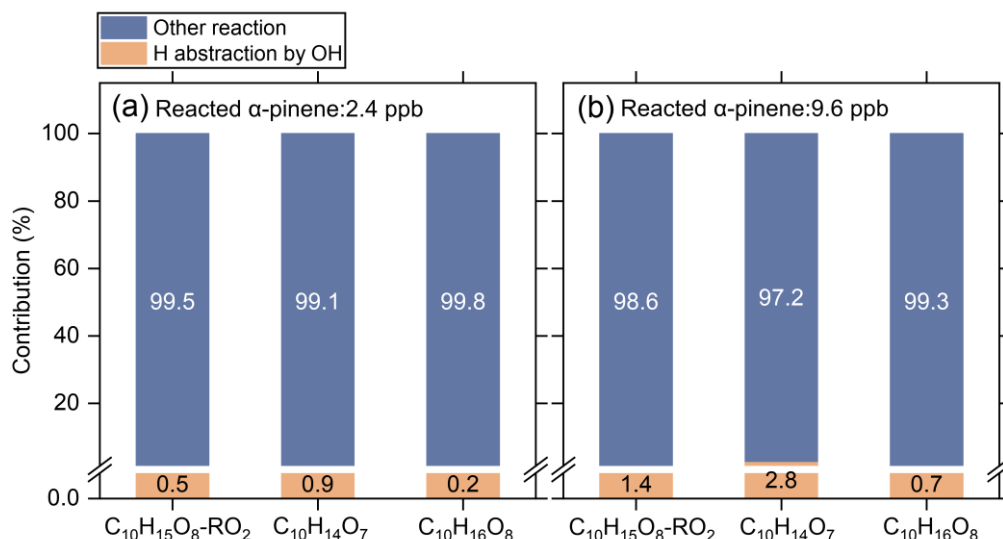
365  
 366 Figure 5 Averaged normalized concentration-signal of typical acyl RO<sub>2</sub> as a function of initial NO  
 367 or NO<sub>2</sub> addition (Exps 1-28 and 33-56).

368 It is interesting to note that most of the measured highly oxygenated acyl RO<sub>2</sub> are formed by the

369 autoxidation of aldehydic RO<sub>2</sub>, and only the C<sub>8</sub>H<sub>13</sub>O<sub>9</sub>-RO<sub>2</sub> is formed by the H-shift of the RO radical  
370 (Figure S9S1104). The ~~measured concentration signal~~ of acyl RO<sub>2</sub> from the autoxidation pathway  
371 accounts for 96% of all highly oxygenated acyl RO<sub>2</sub> ~~concentration signals~~. Considering that the  
372 acyl RO<sub>2</sub> with small molecular size are generally the ring-opened RO<sub>2</sub>, the autoxidation rate constant  
373 of their precursor RO<sub>2</sub> is expected to be relatively high (e.g., 1 s<sup>-1</sup>) (Iyer et al. 2021). Taking a RO<sub>2</sub>  
374 cross-reaction rate constant of 1 × 10<sup>-12</sup> cm<sup>3</sup> molecule<sup>-1</sup> s<sup>-1</sup> (Zhao et al. 2018) and a model-predicted  
375 total RO<sub>2</sub> concentration of 1.7 ppb (Exp 8), ~~the simulated contributions of~~ autoxidation and cross-  
376 reactions ~~contribute to 96.0% and 4.0% of the total RO<sub>2</sub> reaction~~ are 96.0% and 4.0%, respectively.  
377 Considering a 10 times larger RO<sub>2</sub> cross-reaction rate constant (i.e., 1 × 10<sup>-11</sup> cm<sup>3</sup> molecule<sup>-1</sup> s<sup>-1</sup>),  
378 the simulated contributions of RO<sub>2</sub> autoxidation and cross-reactions would be 70.4% and 29.6%,  
379 respectively. These ~~calculations simulations~~ suggest that the autoxidation of aldehydic RO<sub>2</sub> plays a  
380 dominant role in the formation of the highly oxygenated acyl RO<sub>2</sub>. Although the acyl RO<sub>2</sub> with low  
381 oxygen content were not measured in this study, all acyl RO<sub>2</sub> containing oxygen atoms less than 6  
382 seem to be derived from the cleavage of C-C bond or H-shift of RO containing an α-ketone or  
383 aldehyde in the currently known reaction mechanisms (Figures 4 and S10S1212).

384 Recently, Shen et al. (2022) found that the hydrogen abstraction by OH radicals during α-pinene  
385 oxidation plays an important role in HOM formation. In such mechanisms, the primary RO<sub>2</sub> reacts  
386 with NO and forms RO radicals, which could undergo rapid ring-breaking reactions to form a series  
387 of ring-opened C<sub>10</sub>H<sub>15</sub>O<sub>x</sub>-RO<sub>2</sub>, which contains aldehyde functionality and can easily autoxidize to  
388 C<sub>10</sub> acyl RO<sub>2</sub>. In the absence of NO, the cross-reactions of RO<sub>2</sub> can also produce RO radicals.  
389 However, only a few C<sub>10</sub> acyl RO<sub>2</sub> were detected in this study and they contribute less than 1% of  
390 the total C<sub>10</sub> RO<sub>2</sub> concentration. This phenomenon could be due to the fact that the primary RO<sub>2</sub>  
391 (C<sub>10</sub>H<sub>15</sub>O<sub>2</sub>) formed by the hydrogen abstraction by OH radical are least-oxidized with only 2 oxygen  
392 atoms, which are expected to have a relatively low cross-reaction rate constant (Berndt et al. 2018,  
393 Orlando and Tyndall 2012). As a result, the formation of ring-opened C<sub>10</sub>H<sub>15</sub>O<sub>x</sub>-RO<sub>2</sub> via cross-  
394 reactions of the primary C<sub>10</sub>H<sub>15</sub>O<sub>2</sub>-RO<sub>2</sub> may not be important. As shown in Figure 6, when the cross-  
395 reaction rate constants of C<sub>10</sub>H<sub>15</sub>O<sub>2</sub>-RO<sub>2</sub> is considered to be 1 × 10<sup>-13</sup> cm<sup>3</sup> molecule<sup>-1</sup> s<sup>-1</sup>, the  
396 simulated contribution of the H-abstraction pathway to the HOM formation is less than 3% under  
397 both low (2.4 ppb) and high (9.6 ppb) reacted α-pinene conditions. It should be note that the cross-  
398 reaction rate constants of the less-oxygenated RO<sub>2</sub> could be even lower (Orlando and Tyndall 2012),  
399 therefore the contribution of this pathway to HOM formation could be ignored when NO is absent.

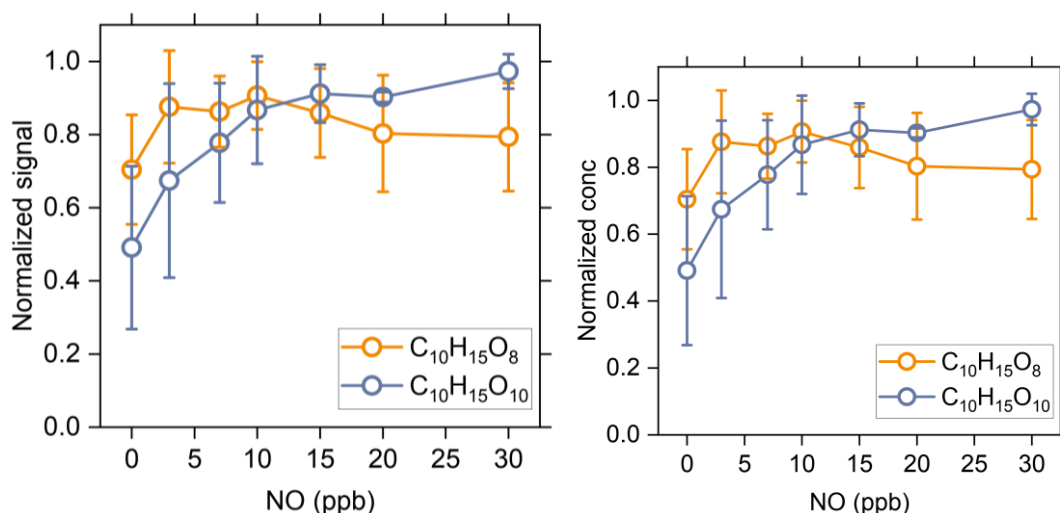




400

401 Figure 6 Contributions of the H-abstraction pathways by OH radicals (yellow) and OH addition and  
 402 ozonolysis pathways (blue) to the formation of typical HOMs under low (a) and high (b) reacted  $\alpha$ -  
 403 pinene conditions simulated by the kinetic model. The cross-reaction rate constant was set to  $1 \times$   
 404  $10^{-13} \text{ cm}^3 \text{ molecule}^{-1} \text{ s}^{-1}$  for the primary C<sub>10</sub>H<sub>15</sub>O<sub>2</sub>-RO<sub>2</sub> and  $1 \times 10^{-12} \text{ cm}^3 \text{ molecule}^{-1} \text{ s}^{-1}$  for the more  
 405 oxygenated RO<sub>2</sub>.

406 In the presence of cyclohexane as an OH scavenger (Figure S11S1323, Exp 32), the measured  
 407 concentrations-signals of C<sub>10</sub>H<sub>17</sub>O<sub>x</sub>-RO<sub>2</sub> formed via OH addition channel and the corresponding  
 408 C<sub>10</sub>H<sub>18</sub>O<sub>x</sub>-HOMs decrease by more than 70%, while the C<sub>10</sub>H<sub>15</sub>O<sub>x</sub>-RO<sub>2</sub> and its related closed-shell  
 409 products decrease by less than 15%, in good agreement with the measurements in previous studies  
 410 (Zhao et al. 2018). As the C<sub>10</sub>H<sub>16</sub>O<sub>8</sub>-HOM could come from both C<sub>10</sub>H<sub>15</sub>O<sub>x</sub>-RO<sub>2</sub> and C<sub>10</sub>H<sub>17</sub>O<sub>x</sub>-RO<sub>2</sub>,  
 411 its reduction is at a medium level. The significantly smaller decrease in the concentrations-signals  
 412 of C<sub>10</sub>H<sub>15</sub>O<sub>x</sub>-RO<sub>2</sub> and its corresponding closed-shell products as compared to those of C<sub>10</sub>H<sub>17</sub>O<sub>x</sub>-  
 413 RO<sub>2</sub> and the related closed-shell products further illustrates that the H-abstraction by OH has a minor  
 414 contribution to HOM formation in the absence of NO.



415

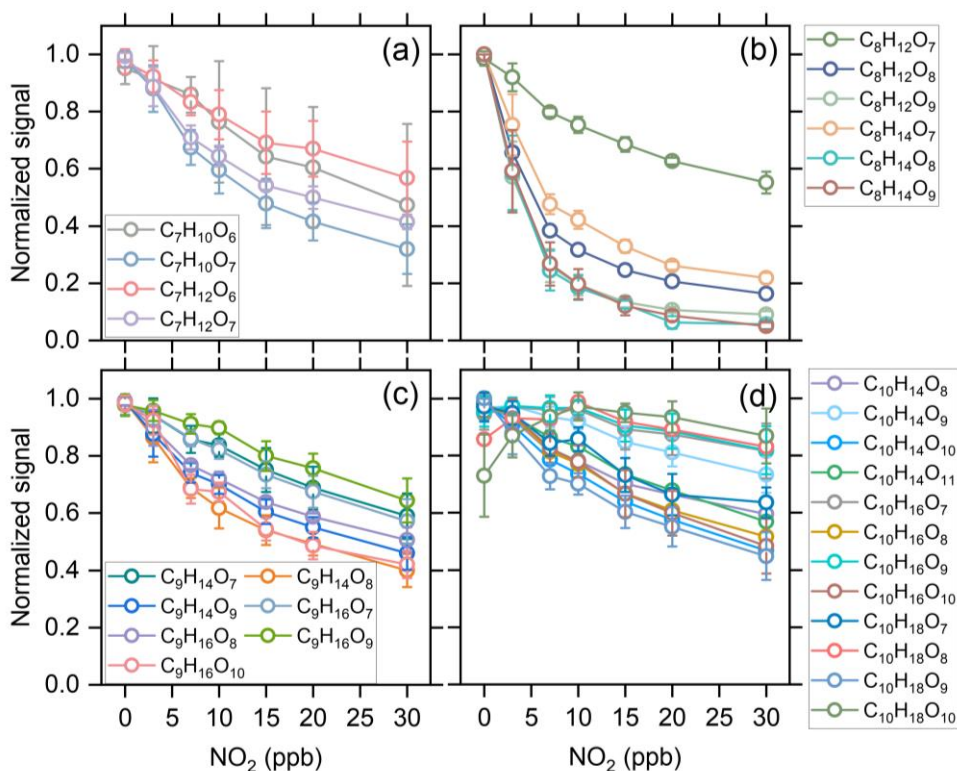
416 Figure 7 Averaged normalized concentration-signal of the measured C<sub>10</sub>H<sub>15</sub>O<sub>8</sub>- and C<sub>10</sub>H<sub>15</sub>O<sub>10</sub>-  
 417 RO<sub>2</sub> as a function of the added NO concentration (Exps 33-56).

418 Figure 7 shows the changes in measured concentration-signal of C<sub>10</sub>H<sub>15</sub>O<sub>8</sub>-RO<sub>2</sub> and C<sub>10</sub>H<sub>15</sub>O<sub>10</sub>-RO<sub>2</sub>  
 419 as a function of initial NO concentration (Exps 33-56). It should be noted that due to the existence  
 420 of O<sub>3</sub> in our experiments, these two RO<sub>2</sub> could come from both O<sub>3</sub> and OH reactions with α-pinene  
 421 and NO could be rapidly oxidized to NO<sub>2</sub> by O<sub>3</sub>. The normalized concentrations-signals of  
 422 C<sub>10</sub>H<sub>15</sub>O<sub>8</sub>-RO<sub>2</sub> and C<sub>10</sub>H<sub>15</sub>O<sub>10</sub>-RO<sub>2</sub> increase firstly under low NO conditions, which is similar to the  
 423 change of acyl RO<sub>2</sub> as shown in Figure 5. This increase could be due to two reasons: (1) the  
 424 promoted formation of C<sub>10</sub>H<sub>15</sub>O<sub>8</sub> and C<sub>10</sub>H<sub>15</sub>O<sub>10</sub> acyl RO<sub>2</sub> from the H-abstraction channel by NO  
 425 addition and (2) the equilibrium decomposition of ROONO<sub>2</sub> formed by the two alkyl RO<sub>2</sub> from  
 426 ozonolysis of α-pinene in the CI inlet (see Section 3.1). As mentioned above, the ring-opened  
 427 C<sub>10</sub>H<sub>15</sub>O<sub>x</sub>-RO<sub>2</sub> formed from the H-abstraction channel contain aldehyde functionality and can  
 428 autoxidize rapidly. The F0AM model simulations show that the C<sub>10</sub>H<sub>15</sub>O<sub>8</sub> and C<sub>10</sub>H<sub>15</sub>O<sub>10</sub> acyl RO<sub>2</sub>  
 429 formed from the H-abstraction channel contribute to 68% and 56% of the total C<sub>10</sub>H<sub>15</sub>O<sub>8</sub>-RO<sub>2</sub> and  
 430 C<sub>10</sub>H<sub>15</sub>O<sub>10</sub>-RO<sub>2</sub> with the addition of 10 ppb NO, respectively. Therefore, the initial increases of these  
 431 two RO<sub>2</sub> with increasing NO concentration are likely mainly due to the enhanced formation of  
 432 C<sub>10</sub>H<sub>15</sub>O<sub>8</sub> and C<sub>10</sub>H<sub>15</sub>O<sub>10</sub> acyl RO<sub>2</sub>. When the NO concentration increases to a high level, there are  
 433 more NO and NO<sub>2</sub> in the system, which promotes the consumption of acyl RO<sub>2</sub>. As a result,  
 434 C<sub>10</sub>H<sub>15</sub>O<sub>8</sub>-RO<sub>2</sub> exhibits a decreasing trend and the increasing extend of C<sub>10</sub>H<sub>15</sub>O<sub>10</sub>-RO<sub>2</sub> becomes  
 435 much smaller.

### 436 3.3 Contributions of acyl RO<sub>2</sub> to the formation of gas-phase HOMs

437 With the addition of NO<sub>2</sub>, the distribution of gas-phase products in the α-pinene ozonolysis changes  
 438 significantly (see Figure 1), and the consumption of acyl RO<sub>2</sub> by NO<sub>2</sub> plays an important role. NO<sub>2</sub>

439 influences the formation of HOM monomers mainly in three ways. Firstly,  $\text{NO}_2$  could react rapidly  
 440 with acyl  $\text{RO}_2$  and form  $\text{RC(O)OONO}_2$ , thus inhibiting the formation of HOMs with the  
 441 involvement of acyl  $\text{RO}_2$ . Secondly, as mentioned above, although  $\text{ROONO}_2$  is thermally unstable,  
 442 their formation/decomposition equilibrium still consumes a small amount of alkyl  $\text{RO}_2$ , resulting in  
 443 a decrease in HOM formation. Thirdly,  $\text{NO}_2$  can consume a part of  $\text{HO}_2$  radicals (Figure S12S1434,  
 444 thus inhibiting the  $\text{RO}_2 + \text{HO}_2$  reaction pathway.



445  
 446 Figure 8 Averaged normalized concentration-signal of the measured  $\text{C}_7$ - $\text{C}_{10}$  HOMs as a function of  
 447 the added  $\text{NO}_2$  concentration (Exps 1-28).

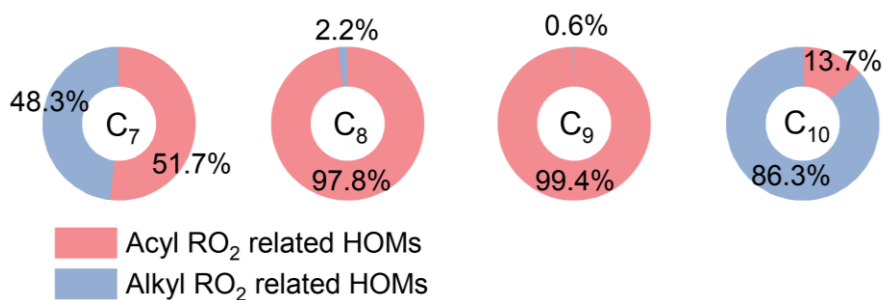
448 Figure 8 shows the normalized concentration-signal of  $\text{C}_7$ - $\text{C}_{10}$  HOM monomers as a function of  
 449 initial  $\text{NO}_2$  concentration. The  $\text{C}_7$ ,  $\text{C}_8$ , and some of  $\text{C}_9$  HOMs decrease significantly with increasing  
 450  $\text{NO}_2$  concentration due to the relatively large contribution of acyl  $\text{RO}_2$  to the total  $\text{C}_7$ - $\text{C}_9$   $\text{RO}_2$ . The  
 451  $\text{C}_7$  HOMs decrease by more than 50% when the  $\text{NO}_2$  concentration reaches 30 ppb, while  $\text{C}_8$  HOMs  
 452 decrease by more than 70% and some of them even decrease by 90%. The  $\text{C}_9$  HOMs decrease by  
 453 30%-60% and the species with relatively large decrease are mostly acyl  $\text{RO}_2$ -related HOMs. For  
 454  $\text{C}_{10}$  HOMs, although there is also an obvious decrease in their formation with the addition of  $\text{NO}_2$ ,  
 455 most of them have a smaller decreasing extent compared to the  $\text{C}_7$ - $\text{C}_9$  HOMs due to the low  
 456 contribution of acyl  $\text{RO}_2$  to the  $\text{C}_{10}$   $\text{RO}_2$ . It is worth noting that a few  $\text{C}_{10}$  HOMs increase initially  
 457 with the addition of  $\text{NO}_2$  up to 10 ppb, suggesting that there might be some processes that promote  
 458 the formation of their precursor  $\text{RO}_2$  radicals and thus offset the inhibiting effect of  $\text{NO}_2$ .

459 As mentioned above, the addition of NO<sub>2</sub> has the most significant influence on the formation of  
460 small HOM monomers. Combined with the large contribution (67-94%) of acyl RO<sub>2</sub> to the total C<sub>7</sub>  
461 and C<sub>8</sub> RO<sub>2</sub> (Figure 3), it can be considered that the reduction in the formation of C<sub>7</sub> and C<sub>8</sub> HOM  
462 monomers with NO<sub>2</sub> addition is overwhelmingly due to the consumption of acyl RO<sub>2</sub> by NO<sub>2</sub>. As a  
463 result, acyl RO<sub>2</sub> was found to have a contribution of 50-90% to C<sub>7</sub> and C<sub>8</sub> HOM monomer formation  
464 during  $\alpha$ -pinene ozonolysis. Since acyl RO<sub>2</sub> also have a considerable contribution (32%) to the total  
465 C<sub>9</sub> RO<sub>2</sub>, an upper limit (30%-60%) of its contribution to C<sub>9</sub> HOMs could be derived with the  
466 assumption that the decrease of C<sub>9</sub> HOMs with the addition of NO<sub>2</sub> is also mainly due to the  
467 consumption of C<sub>9</sub>-acyl RO<sub>2</sub> by NO<sub>2</sub>. By contrast, acyl RO<sub>2</sub> account for a very small fraction (0.54%)  
468 of the total C<sub>10</sub> RO<sub>2</sub>, and their contribution to C<sub>10</sub> HOMs cannot be quantified based solely on the  
469 experimental measurements given that the equilibrium reaction between alkyl RO<sub>2</sub> and NO<sub>2</sub> can  
470 also affect the formation of HOMs. Therefore, we used the FOAM model to simulate the contribution  
471 of acyl RO<sub>2</sub> to C<sub>10</sub> HOM formation according to the acyl RO<sub>2</sub> measured in this study and displayed  
472 the results in Figure 9. It should be noted that the HOMs from the acyl RO<sub>2</sub> and its subsequent RO<sub>2</sub>  
473 (formed from acyl RO<sub>2</sub> reactions) are all considered as acyl RO<sub>2</sub>-related HOMs in the model.

474 As mentioned above, the formation of ring-opened C<sub>10</sub>H<sub>15</sub>O<sub>4</sub>-RO<sub>2</sub> reported by Iyer et al. (2021) is  
475 included in the model, and its autoxidation produces a ring-opened acyl C<sub>10</sub>H<sub>15</sub>O<sub>8</sub>-RO<sub>2</sub>. When we  
476 considered the upper limit of the yield of ring-opened C<sub>10</sub>H<sub>15</sub>O<sub>4</sub>-RO<sub>2</sub> (89%) in the model and  
477 assumes that the other primary RO<sub>2</sub> with the cyclobutyl ring autoxidize at a very slow rate (0.01 s<sup>-1</sup>),  
478 the simulated acyl C<sub>10</sub>H<sub>15</sub>O<sub>8</sub>-RO<sub>2</sub> would contribute to ~80% of the total C<sub>10</sub> RO<sub>2</sub>. However, we  
479 could not see a large decrease in the measured ~~concentration-signal~~ of C<sub>10</sub>H<sub>15</sub>O<sub>8</sub>-RO<sub>2</sub> and its related  
480 HOM monomers with the addition of NO<sub>2</sub>. Similarly, a recent study by Zhao et al. (2022) found  
481 that the C<sub>10</sub>H<sub>15</sub>O<sub>8</sub>-related monomers and dimers in  $\alpha$ -pinene SOA ~~also~~ did not ~~show~~ significantly  
482 decreases with NO<sub>2</sub> addition. There might be ~~two~~-~~three~~ reasons for the discrepancy between the  
483 simulations and measurements. Firstly, the yield of the ring-opened C<sub>10</sub>H<sub>15</sub>O<sub>4</sub>-RO<sub>2</sub> might be  
484 significantly smaller than 89% (Wang et al. 2021, Meder et al. 2023). Secondly, the autoxidation  
485 rate of other primary C<sub>10</sub>H<sub>15</sub>O<sub>4</sub>-RO<sub>2</sub> with the cyclobutyl ring could be significantly larger than 0.01  
486 s<sup>-1</sup>. Thirdly, the ring-opened C<sub>10</sub>H<sub>15</sub>O<sub>8</sub>-RO<sub>2</sub>, a highly functionalized acyl RO<sub>2</sub> radical with an -OOH  
487 group, may be able to undergo very fast intramolecular H-scrambling reactions to form a peroxy  
488 acid as suggested by Knap and Jørgensen (2017), which would compete with the NO<sub>2</sub> reaction and  
489 result in a lower reduction in its signal upon NO<sub>2</sub> addition (see details in Section S3).

490 To examine the contributions of acyl RO<sub>2</sub> to C<sub>10</sub> HOM production, ~~We~~ updated the branching  
491 ratios and autoxidation rates of the primary RO<sub>2</sub> during ~~the~~  $\alpha$ -pinene ozonolysis in the model

492 according to the recent studies (Wang et al. 2021, Kurten et al. 2015, Claffin et al. 2018, Berndt  
 493 2022) (Table S3), and used a lower limit (30%) of the ring-opened  $C_{10}H_{15}O_4-RO_2$  yield reported by  
 494 Iyer et al. (2021) ~~was used here~~. The simulated acyl  $RO_2$ -related HOMs contribute to 14% of the  
 495 total  $C_{10}$  HOMs, which is slightly smaller than the measured decrease in  $C_{10}$  HOMs with the addition  
 496 of  $NO_2$ . This discrepancy could be due to two reasons. Firstly, the decrease in HOMs can partly  
 497 result from the consumption of alkyl  $RO_2$  and  $HO_2$  radicals by the addition of  $NO_2$ . Secondly, as  
 498 mentioned above, there might be other  $C_{10}$  acyl  $RO_2$  that were not observed in this study due to the  
 499 decomposition of the  $ROONO_2$  from the alkyl  $RO_2$  with the same formulas. The contributions of  
 500 acyl  $RO_2$  to the formation of  $C_7$ - $C_9$  HOMs were also simulated (Figure 9). For  $C_7$  and  $C_8$  HOMs,  
 501 the model predicts a contribution of 52%-98% from acyl  $RO_2$ , which is consistent with the  
 502 measurements (50%-90%). However, the simulated contribution of acyl  $RO_2$  to  $C_9$  HOMs is over  
 503 99%, which is not consistent with the measurements (Figure 8c). Recent studies indicated that the  
 504 CI radicals from  $\alpha$ -pinene ozonolysis could not form the alkyl  $C_9H_{15}O_3-RO_2$  ( $C_9O_2$  in default  
 505 MCM v3.3.1) (Berndt 2022, Wang et al. 2021, Kurten et al. 2015). As a result, this primary  $C_9$  alkyl  
 506  $RO_2$  was not considered in the model, and most of  $C_9$   $RO_2$  considered are acyl  $RO_2$  or from acyl  
 507  $RO_2$  reactions. In view of the significantly lower measured (less than 30-60%) than simulated (over  
 508 99%) contribution of acyl  $RO_2$  to  $C_9$  HOMs, we speculate that a small part of CI radicals might be  
 509 able to form the  $C_9H_{15}O_3-RO_2$ , which could further react to form highly oxygenated alkyl  $C_9$   $RO_2$ .



510  
 511 Figure 9 Simulated average contribution of acyl and alkyl  $RO_2$  to  $C_7$ - $C_{10}$  HOM formation from  
 512 ozonolysis of  $\alpha$ -pinene under typical experimental conditions (Exps 1, 8, 15, and 22).

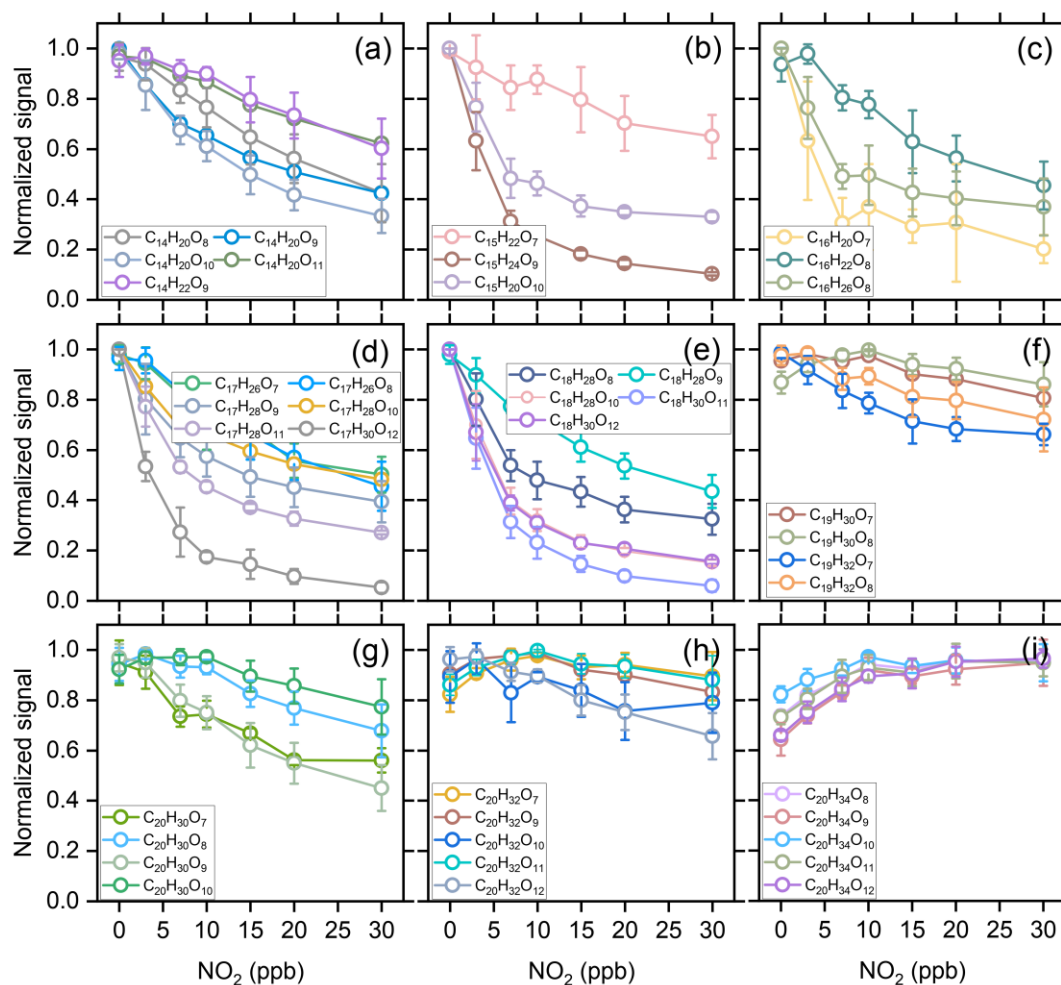
513  
 514 A sensitive-sensitivity analysis of the alkyl  $C_9H_{15}O_3-RO_2$  yield was conducted to see its influence  
 515 on the contribution of acyl  $RO_2$  to the total  $C_9$  HOMs. The model simulations show that when the  
 516 yield of this  $C_9$   $RO_2$  from one of the CIs ranges between 0.5% to 2%, the contribution of acyl  $RO_2$   
 517 to the total  $C_9$  HOMs ranges from 27.5% to 59.8% (Figure ~~S13~~S155), which is almost consistent  
 518 with the measurements. This result indicates that a small part of CIs could generate the  $C_9$  alkyl  
 519  $RO_2$ . We note that Wethe small production of  $C_9H_{15}O_3-RO_2$  from CIs has no significant influence

520 on the yield of  $C_{10}H_{15}O_4-RO_2$  and the subsequent acyl  $RO_2$ . As shown in Figure S16, as the  $C_9H_{15}O_3-$   
521  $RO_2$  yield increases from 0% to 3%, the simulated concentrations of  $C_{10}H_{15}O_4-RO_2$  exhibit  
522 negligible to small (5%) changes. As the  $C_9H_{15}O_3-RO_2$  is considered to only produce highly  
523 oxygenated alkyl  $RO_2$  in the model, it results in a decrease in the contribution of acyl  $RO_2$  to the  
524 total  $C_9$  HOMs. However, the contributions of acyl  $RO_2$  to total  $C_7$ ,  $C_8$ , and  $C_{10}$  HOMs are almost  
525 unchanged.

526 The cross-reaction rate constant of acyl  $RO_2$  is generally larger than that of alkyl  $RO_2$  (Orlando and  
527 Tyndall 2012, Atkinson et al. 2007), and the fast cross-reaction may lead to an important  
528 contribution to the HOM dimer production. The responses of dimer formation to increasing  
529 concentration of initial  $NO_2$  during  $\alpha$ -pinene ozonolysis are given in Figure 10. The  $C_{14}$ - $C_{18}$  dimers  
530 decrease by up to 50%-95% with the increase of  $NO_2$  concentration up to 30 ppb (Figures 10a-e).  
531 The rapid cross-reaction rate of acyl  $RO_2$ , as well as their dominant contribution to the small  $RO_2$   
532 species makes acyl  $RO_2$  an important contributor to the formation of these dimers. The consumption  
533 of acyl  $RO_2$  by  $NO_2$  greatly inhibits the bimolecular reactions involving acyl  $RO_2$ , resulting in a  
534 rapid decrease in the ~~concentration~~-signal of the corresponding dimers. Considering the  
535 predominance of acyl  $RO_2$  in small  $RO_2$  and their high reaction rate with  $NO_2$  compared to the alkyl  
536  $RO_2$ , it can be concluded that the cross-reactions involving acyl  $RO_2$  contribute to roughly 50%-95%  
537 of the  $C_{14}$ - $C_{18}$  dimer formation.

538 For  $C_{19}$  dimers, due to the relatively smaller contribution of acyl  $RO_2$  to  $C_9$  and  $C_{10}$   $RO_2$ , their  
539 ~~concentration~~-signal decreases only by 10%-40%, and this reduction have contributions from both  
540 acyl and alkyl  $RO_2$ . For  $C_{20}$  dimers, their ~~concentration~~-signal changes with the addition of  $NO_2$  can  
541 be discussed according to the number of hydrogen atoms in the molecules. Firstly, the ~~concentration~~  
542 signal of  $C_{20}H_{30}O_7$  and  $C_{20}H_{30}O_9$  decreases by 40-60% with the addition of 30 ppb  $NO_2$ , indicating  
543 a significant contribution of acyl  $RO_2$  such as  $C_{10}H_{15}O_5-RO_2$  (acyl  $RO_2$  in default MCM v3.3.1) and  
544  $C_{10}H_{15}O_7-RO_2$  in their formation, while other  $C_{20}H_{30}O_x$  dimers decrease by ~30%. The  $C_{20}H_{32}O_x$   
545 dimer series also exhibits a small reduction (less than 20%) with the addition of  $NO_2$ . However, the  
546  $C_{20}H_{34}O_x$  series shows an unexpected increase with the addition of  $NO_2$  up to 10 ppb and almost  
547 remains unchanged with the further increase of  $NO_2$  concentration. Given that the cross-reaction  
548 rate constant of acyl  $RO_2$  can be orders of magnitude higher than that of counterpart alkyl  $RO_2$   
549 (Orlando and Tyndall 2012, Atkinson et al. 2007), the rapid consumption of acyl  $RO_2$  by  $NO_2$  would  
550 preserve the alkyl  $RO_2$  that tend to react with acyl  $RO_2$  at a fast rate in the absence of  $NO_2$ , which  
551 to some extent would elevate the concentration of alkyl  $RO_2$  in the system and thus promote the less  
552 competitive alkyl  $RO_2 +$  alkyl  $RO_2$  reactions to form  $C_{20}H_{34}O_x$  dimers. The slight increase of some

553 C<sub>10</sub>H<sub>18</sub>O<sub>x</sub>-HOMs with the addition of NO<sub>2</sub> up to 10 ppb could also be due to this reason.

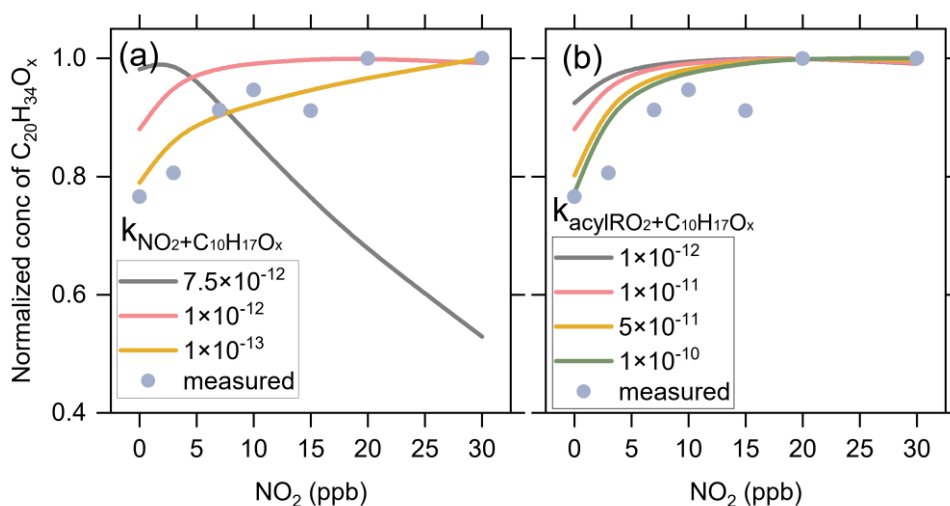


554  
555 Figure 10 Averaged normalized concentration-signal of the measured C<sub>14</sub>-C<sub>20</sub> dimers as a function  
556 of the added NO<sub>2</sub> concentration (Exps 1-28).

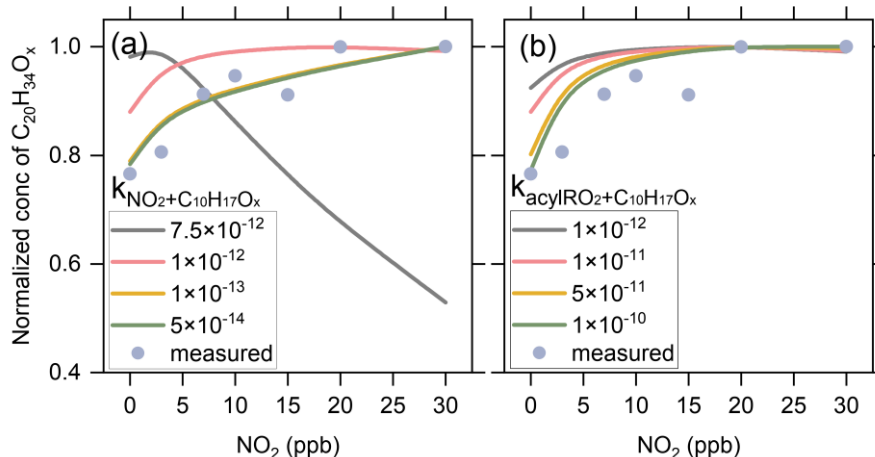
557 According to the noticeable increasing trend in C<sub>20</sub>H<sub>34</sub>O<sub>x</sub> as compared to other C<sub>20</sub> dimers, we  
558 speculate that acyl RO<sub>2</sub> react faster with C<sub>10</sub>H<sub>17</sub>O<sub>x</sub> alkyl RO<sub>2</sub> than with C<sub>10</sub>H<sub>15</sub>O<sub>x</sub> alkyl RO<sub>2</sub>.  
559 Therefore, when the acyl RO<sub>2</sub> is depleted, the preservation of C<sub>10</sub>H<sub>17</sub>O<sub>x</sub>-RO<sub>2</sub> is more significant and  
560 the promotion of their cross-reactions to form C<sub>20</sub>H<sub>34</sub>O<sub>x</sub> is more evident. It is also possible that the  
561 reaction of NO<sub>2</sub> with C<sub>10</sub>H<sub>17</sub>O<sub>x</sub> alkyl RO<sub>2</sub> is less efficient compared to the reaction with C<sub>10</sub>H<sub>15</sub>O<sub>x</sub>  
562 alkyl RO<sub>2</sub>, so more C<sub>10</sub>H<sub>17</sub>O<sub>x</sub> than C<sub>10</sub>H<sub>15</sub>O<sub>x</sub> are available for dimer formation in the presence of  
563 NO<sub>2</sub>.

564 To further prove the above two speculations, we performed sensitivity analyses for the reaction rates  
565 of C<sub>10</sub>H<sub>17</sub>O<sub>x</sub>-RO<sub>2</sub> using the F0AM model. Figures 11a show the changes in C<sub>20</sub>H<sub>34</sub>O<sub>x</sub> dimers with  
566 NO<sub>2</sub> addition at different C<sub>10</sub>H<sub>17</sub>O<sub>x</sub>-RO<sub>2</sub> + NO<sub>2</sub> reaction rates under the conditions of Exps 8-14. As  
567 the reaction rate varies from  $5.1 \times 10^{-14}$  to  $1 \times 10^{-12}$  cm<sup>3</sup> molecule<sup>-1</sup> s<sup>-1</sup>, the increasing trend of

568  $C_{20}H_{34}O_x$  dimers versus the added  $NO_2$  concentration is significantly weakened and the simulations  
 569 are is more deviated from the measurements. When the reaction rate increases to  $7.5 \times 10^{-12} \text{ cm}^3$   
 570  $\text{molecule}^{-1} \text{ s}^{-1}$ , the  $C_{20}H_{34}O_x$  dimers decrease significantly with increasing  $NO_2$ , which is in striking  
 571 contrast to the measurements. Figure 11b presents the sensitivity analysis results for the cross-  
 572 reaction rate constants of acyl  $RO_2 + C_{10}H_{17}O_x-RO_2$ . As this rate constant varies from  $1 \times 10^{-12}$  to  $1$   
 573  $\times 10^{-10} \text{ cm}^3 \text{ molecule}^{-1} \text{ s}^{-1}$ , the increasing trend of  $C_{20}H_{34}O_x$  versus the  $NO_2$  concentration is more  
 574 pronounced and more consistent with the measurements. These sensitivity analyses support our  
 575 speculation that the  $C_{10}H_{17}O_x$  alkyl  $RO_2$  may be different from other alkyl  $RO_2$  radicals in terms of  
 576 the reaction efficiency with  $NO_2$  and acyl  $RO_2$  species, which leads to different responses of  
 577  $C_{20}H_{34}O_x$  dimers to  $NO_2$  addition compared to other  $C_{20}$  dimers. These results also suggest that the  
 578 presence of acyl  $RO_2$  could affect the fate and contribution of alkyl  $RO_2$  to HOM formation in  
 579 atmospheric oxidation systems given the different reactivity of acyl  $RO_2$  from alkyl  $RO_2$ .



580



581

582 Figure 11 Sensitivity analyses of  $C_{20}H_{34}O_x$  dimer production to (a) the reaction rates of  $NO_2$  with  
 583  $C_{10}H_{17}O_x-RO_2$  (a), and (b) the cross-reaction rate of acyl  $RO_2$  with  $C_{10}H_{17}O_x-RO_2$  (b), considering



584 a  $C_{10}H_{17}O_x-RO_2 + NO_2$  reaction rate of  $1 \times 10^{-12}$  cm<sup>3</sup> molecule<sup>-1</sup> s<sup>-1</sup> for  $C_{10}H_{17}O_x-RO_2 + NO_2$ .

#### 585 4. Conclusions

586 In this study, the molecular identities, formation mechanisms, and contributions of acyl RO<sub>2</sub> to the  
587 formation of HOMs during ozonolysis of  $\alpha$ -pinene are investigated using a combination of flow  
588 reactor experiments and detailed kinetic model simulations. Based on the marked decrease in RO<sub>2</sub>  
589 ~~concentration-signal~~ as a function of initial NO<sub>2</sub> concentration, a total of 10 acyl RO<sub>2</sub> are identified  
590 during  $\alpha$ -pinene ozonolysis. The acyl RO<sub>2</sub> contributes to 67%, 94% and 32% of C<sub>7</sub>, C<sub>8</sub> and C<sub>9</sub> highly  
591 oxygenated RO<sub>2</sub> but only 0.45% of C<sub>10</sub> highly oxygenated RO<sub>2</sub>, respectively. Three main pathways  
592 are identified for the formation of monoterpene-derived acyl RO<sub>2</sub>: (i) the autoxidation of RO<sub>2</sub>  
593 containing aldehyde groups, (ii) the cleavage of C-C bond of RO containing an  $\alpha$ -ketone group, and  
594 (iii) the intramolecular H-shift of RO containing an aldehyde group. The autoxidation of aldehydic  
595 RO<sub>2</sub> formed involving multiple RO decomposition or ring-opening steps plays a dominant role in  
596 the formation of the highly oxygenated acyl RO<sub>2</sub> radicals (oxygen atom number  $\geq 6$ ), while the  
597 less-oxygenated acyl RO<sub>2</sub> (oxygen atom number  $< 6$ ) are mainly derived from the other two  
598 pathways.

599 The acyl RO<sub>2</sub>-involved reactions explain 50-90% of C<sub>7</sub> and C<sub>8</sub> HOM monomers and 14% of C<sub>10</sub>  
600 HOMs, respectively. For C<sub>9</sub> HOMs, this contribution can be up to 30%-60%. For the HOM dimers,  
601 acyl RO<sub>2</sub>-involved reactions contribute 50%-95% to the formation of C<sub>14</sub>-C<sub>18</sub> dimers. Owing to the  
602 higher cross-reaction rate constant of acyl RO<sub>2</sub> compared to alkyl RO<sub>2</sub>, the acyl RO<sub>2</sub> + alkyl RO<sub>2</sub>  
603 reaction would outcompete the alkyl RO<sub>2</sub> + alkyl RO<sub>2</sub> reaction. Therefore, the rapid consumption  
604 of acyl RO<sub>2</sub> by NO<sub>2</sub> in the experiments (as well as in polluted atmospheres) would make the alkyl  
605 RO<sub>2</sub> that are supposed to react with acyl RO<sub>2</sub> retained, which to some extent elevates the  
606 concentration of alkyl RO<sub>2</sub> in the system and thus promotes the reaction of alkyl RO<sub>2</sub> + alkyl RO<sub>2</sub>  
607 to form dimers such as C<sub>20</sub>H<sub>34</sub>O<sub>x</sub>. The contribution of H-abstraction of  $\alpha$ -pinene by OH radical to  
608 the formation of acyl RO<sub>2</sub> and HOMs is found to be negligible in the absence of NO. This is because  
609 the primary C<sub>10</sub>H<sub>15</sub>O<sub>2</sub>-RO<sub>2</sub> radicals formed in such pathways are least-oxidized and thus have  
610 relatively low cross-reaction efficiency to produce RO radicals, which are the key intermediates for  
611 the formation of acyl RO<sub>2</sub> and HOMs in that channel. However, in the presence of NO, the formation  
612 of highly oxygenated acyl RO<sub>2</sub> via the H-abstraction pathway is demonstrated, consistent with  
613 previous studies (Shen et al., 2022).

614 In this study, acyl RO<sub>2</sub> species are identified according to a dramatic decrease in their ~~concentration~~  
615 ~~signal~~ with the addition of NO<sub>2</sub>. It should be noted that the presence of NO<sub>2</sub> could also inhibit the  
616 formation of alkyl RO<sub>2</sub> species involving acyl RO<sub>2</sub> reactions. If there are any contributions of alkyl

617 RO<sub>2</sub> to acyl RO<sub>2</sub> identified in this study, the influence of such alkyl RO<sub>2</sub> species on HOM formation  
618 would reflect an indirect effect of acyl RO<sub>2</sub>. However, given that the formation of most of the acyl  
619 RO<sub>2</sub> identified in this study can be reasonably explained by the proposed mechanisms and verified  
620 by their responses to the addition of NO, the acyl RO<sub>2</sub> identified here are expected to have no  
621 significant contributions from alkyl RO<sub>2</sub>. Currently, the reaction kinetics of monoterpene-derived  
622 acyl RO<sub>2</sub> are still poorly understood. Considering the important contribution of acyl RO<sub>2</sub> to HOM  
623 formation, further kinetic studies are needed to get more specific rate constants for their autoxidation  
624 and cross-reactions, thereby deepening our understanding of the role of acyl RO<sub>2</sub> in HOM and SOA  
625 formation under atmospheric conditions.

626

627 *Data availability.* The data presented in this work are available upon request from the corresponding  
628 author.

629

630 *Author contributions.* YZ and HZ designed the study, HZ, DH and JZ performed the experiments.  
631 YZ and HZ analyzed the data, conducted model simulations, and wrote the paper. All other authors  
632 contributed to discussion and writing.

633

634 *Competing interests.* The authors declare no conflict of interest.

635

636 *Acknowledgments.* Yue Zhao acknowledges the Program for Professor of Special  
637 Appointment (Eastern Scholar) at Shanghai Institutions of Higher Learning.

638

639 *Financial support.* This work was supported by the National Natural Science Foundation  
640 of China (grants 22022607, 21806104, and 42005090) and the Program for Professor of  
641 Special Appointment (Eastern Scholar) at Shanghai Institutions of Higher Learning.

642

## 643 **References**

644 Atkinson, R., Hasegawa, D., and Aschmann, S. M.: Rate constants for the gas-phase reactions of O<sub>3</sub> with  
645 a series of monoterpenes and related compounds at 296 ± 2 K, *Int. J. Chem. Kinet.*, 1221,  
646 <https://doi.org/10.1002/kin.550220807>, 1990.

647 Atkinson, R., Baulch, D., Cox, R., Crowley, J., Hampson, R., Hynes, R., Jenkin, M., Rossi, M., and Troe,  
648 J.: Evaluated kinetic and photochemical data for atmospheric chemistry: Volume III—gas phase  
649 reactions of inorganic halogens, *Atmos. Chem. Phys.*, 7, 981-1191, [https://doi.org/10.5194/acp-7-](https://doi.org/10.5194/acp-7-981-2007)  
650 981-2007, 2007.

651 Bell, D. M., Wu, C., Bertrand, A., Graham, E., Schoonbaert, J., Giannoukos, S., Baltensperger, U., Prevot,  
652 A., Riipinen, I., and Haddad, I. E.: Particle-phase processing of α-pinene NO<sub>3</sub> secondary organic  
653 aerosol in the dark, *Atmos. Chem. Phys.*, 13167–13182, [https://doi.org/10.5194/acp-22-13167-](https://doi.org/10.5194/acp-22-13167-2022)  
654 2022, 2021.

655 Berndt, T.: Peroxy radical processes and product formation in the OH radical-initiated oxidation of alpha-

656 pinene for near-atmospheric conditions, *J. Phys. Chem. A*, 125, 9151-9160,  
657 <https://doi.org/10.1021/acs.jpca.1c05576>, 2021.

658 Berndt, T.: Peroxy radical and product formation in the gas-phase ozonolysis of alpha-pinene under near-  
659 atmospheric conditions: occurrence of an additional series of peroxy radicals O<sub>2</sub>O-  
660 C<sub>10</sub>H<sub>15</sub>O(O<sub>2</sub>)<sub>y</sub>O<sub>2</sub> with y = 1-3, *J. Phys. Chem. A*, 126, 6526-6537,  
661 <https://doi.org/10.1021/acs.jpca.2c05094>, 2022.

662 Berndt, T., Mentler, B., Scholz, W., Fischer, L., Herrmann, H., Kulmala, M., and Hansel, A.: Accretion  
663 product formation from ozonolysis and OH radical reaction of alpha-pinene: mechanistic insight  
664 and the influence of isoprene and ethylene, *Environ. Sci. Technol.*, 52, 11069-11077,  
665 <https://doi.org/10.1021/acs.est.8b02210>, 2018.

666 Berndt, T., Richters, S., Jokinen, T., Hyttinen, N., Kurtén, T., Otkjær, R. V., Kjaergaard, H. G., Stratmann,  
667 F., Herrmann, H., and Sipilä, M.: Hydroxyl radical-induced formation of highly oxidized organic  
668 compounds, *Nat. Commun.*, 7, 1-8, <https://doi.org/10.1038/ncomms13677>, 2016.

669 Bianchi, F., Kurtén, T., Riva, M., Mohr, C., Rissanen, M. P., Roldin, P., Berndt, T., Crouse, J. D.,  
670 Wennberg, P. O., and Mentel, T. F.: Highly oxygenated organic molecules (HOM) from gas-phase  
671 autoxidation involving peroxy radicals: A key contributor to atmospheric aerosol, *Chem. Rev.*, 119,  
672 3472-3509, 2019.

673 Calvert, J. G., Derwent, R. G., Orlando, J. J., Wallington, T. J., and Tyndall, G. S.: Mechanisms of  
674 atmospheric oxidation of the alkanes, 2008.

675 Claffin, M. S., Krechmer, J. E., Hu, W., Jimenez, J. L., and Ziemann, P. J.: Functional group composition  
676 of secondary organic aerosol formed from ozonolysis of  $\alpha$ -pinene under high VOC and autoxidation  
677 conditions, *ACS Earth Space Chem.*, 2, 1196-1210,  
678 <https://doi.org/10.1021/acsearthspacechem.8b00117>, 2018.

679 Ehn, M., Thornton, J. A., Kleist, E., Sipilä, M., Junninen, H., Pullinen, I., Springer, M., Rubach, F.,  
680 Tillmann, R., and Lee, B.: A large source of low-volatility secondary organic aerosol, *Nature*, 506,  
681 476-479, <https://doi.org/10.1038/nature13032>, 2014.

682 Fry, J., Kiendler-Scharr, A., Rollins, A., Wooldridge, P., Brown, S., Fuchs, H., Dubé, W., Mensah, A., Dal  
683 Maso, M., and Tillmann, R.: Organic nitrate and secondary organic aerosol yield from NO<sub>3</sub>  
684 oxidation of  $\beta$ -pinene evaluated using a gas-phase kinetics/aerosol partitioning model, *Atmos.*  
685 *Chem. Phys.*, 9, 1431-1449, <https://doi.org/10.5194/acp-9-1431-2009>, 2009.

686 Fry, J. L., Draper, D. C., Barsanti, K. C., Smith, J. N., Ortega, J., Winkler, P. M., Lawler, M. J., Brown,  
687 S. S., Edwards, P. M., and Cohen, R. C.: Secondary organic aerosol formation and organic nitrate  
688 yield from NO<sub>3</sub> oxidation of biogenic hydrocarbons, *Environ. Sci. Technol.*, 48, 11944-11953,  
689 <https://doi.org/10.1021/es502204x>, 2014.

690 Guenther, A., Jiang, X., Heald, C. L., Sakulyanontvittaya, T., Duhl, T. a., Emmons, L., and Wang, X.:  
691 The model of emissions of gases and aerosols from nature version 2.1 (MEGAN2. 1): an extended  
692 and updated framework for modeling biogenic emissions, *Geosci. Model Dev.*, 5, 1471-1492,  
693 <https://doi.org/10.5194/gmd-5-1471-2012>, 2012.

694 Iyer, S., Rissanen, M. P., Valiev, R., Barua, S., Krechmer, J. E., Thornton, J., Ehn, M., and Kurten, T.:  
695 Molecular mechanism for rapid autoxidation in alpha-pinene ozonolysis, *Nat. Commun.*, 12, 878,  
696 <https://doi.org/10.1038/s41467-021-21172-w>, 2021.

697 Jenkin, M., Young, J., and Rickard, A.: The MCM v3.3.1 degradation scheme for isoprene, *Atmos. Chem.*  
698 *Phys.*, 15, 11433-11459, <https://doi.org/10.5194/acp-15-11433-2015>, 2015.

699 Jokinen, T., Sipilä, M., Richters, S., Kerminen, V. M., Paasonen, P., Stratmann, F., Worsnop, D., Kulmala,

700 M., Ehn, M., and Herrmann, H.: Rapid autoxidation forms highly oxidized RO<sub>2</sub> radicals in the  
701 atmosphere, *Angew. Chem. Int. Ed.*, 53, 14596-14600, <https://doi.org/10.1002/anie.201408566>,  
702 2014.

703 Junninen, H., Ehn, M., Petäjä, T., Luosujärvi, L., Kotiaho, T., Kostiainen, R., Rohner, U., Gonin, M.,  
704 Fuhrer, K., and Kulmala, M.: A high-resolution mass spectrometer to measure atmospheric ion  
705 composition, *Atmos. Meas. Tech.*, 3, 599-636, <https://doi.org/10.5194/amt-3-1039-2010>, 2010.

706 Kirchner, F., Thuener, L., Barnes, I., Becker, K., Donner, B., and Zabel, F.: Thermal lifetimes of  
707 peroxy nitrates occurring in the atmospheric degradation of oxygenated fuel additives, *Environ. Sci.*  
708 *Technol.*, 31, 1801-1804, <https://doi.org/10.1021/es9609415>, 1997.

709 [Knap, H. C. and Jørgensen, S.: Rapid Hydrogen Shift Reactions in Acyl Peroxy Radicals, \*J. Phys. Chem.\*  
710 \*A\*, 121, 1470-1479, 10.1021/acs.jpca.6b12787, 2017.](#)

711 Knopf, D. A., Pöschl, U., and Shiraiwa, M.: Radial diffusion and penetration of gas molecules and aerosol  
712 particles through laminar flow reactors, denuders, and sampling tubes, *Anal. Chem.*, 87, 3746-3754,  
713 <https://doi.org/10.1021/ac5042395>, 2015.

714 Kristensen, K., Watne, Å. K., Hammes, J., Lutz, A., Petäjä, T., Hallquist, M., Bilde, M., and Glasius, M.:  
715 High-molecular weight dimer esters are major products in aerosols from  $\alpha$ -pinene ozonolysis and  
716 the boreal forest, *Environ. Sci. Technol. Lett.*, 3, 280-285, 2016.

717 Kurten, T., Rissanen, M. P., Mackeprang, K., Thornton, J. A., Hyttinen, N., Jørgensen, S., Ehn, M., and  
718 Kjaergaard, H. G.: Computational study of hydrogen shifts and ring-opening mechanisms in alpha-  
719 pinene ozonolysis products, *J. Phys. Chem. A*, 119, 11366-11375,  
720 <https://doi.org/10.1021/acs.jpca.5b08948>, 2015.

721 Li, X., Chee, S., Hao, J., Abbatt, J. P. D., Jiang, J., and Smith, J. N.: Relative humidity effect on the  
722 formation of highly oxidized molecules and new particles during monoterpene oxidation, *Atmos.*  
723 *Chem. Phys.*, 19, 1555-1570, <https://doi.org/10.5194/acp-19-1555-2019>, 2019.

724 Lin, C., Huang, R.-J., Duan, J., Zhong, H., and Xu, W.: Primary and secondary organic nitrate in  
725 northwest China: a case study, *Environ. Sci. Technol. Lett.*, 8, 947-953,  
726 <https://doi.org/10.1021/acs.estlett.1c00692>, 2021.

727 Meder, M., Peräkylä, O., Varelas, J. G., Luo, J., Cai, R., Zhang, Y., Kurtén, T., Riva, M., Rissanen, M.,  
728 Geiger, F. M., Thomson, R. J., and Ehn, M.: Selective deuteration as a tool for resolving  
729 autoxidation mechanisms in  $\alpha$ -pinene ozonolysis, *Atmos. Chem. Phys.*, 23, 4373-4390,  
730 <https://doi.org/10.5194/egusphere-2022-1131>, 2023.

731 Mentel, T., Springer, M., Ehn, M., Kleist, E., Pullinen, I., Kurtén, T., Rissanen, M., Wahner, A., and Wildt,  
732 J.: Formation of highly oxidized multifunctional compounds: autoxidation of peroxy radicals  
733 formed in the ozonolysis of alkenes—deduced from structure–product relationships, *Atmos. Chem.*  
734 *Phys.*, 15, 6745-6765, <https://doi.org/10.5194/acp-15-6745-2015>, 2015.

735 Molteni, U., Simon, M., Heinritzi, M., Hoyle, C. R., Bernhammer, A.-K., Bianchi, F., Breitenlechner, M.,  
736 Brilke, S., Dias, A., Duplissy, J., Frege, C., Gordon, H., Heyn, C., Jokinen, T., Kürten, A., Lehtipalo,  
737 K., Makhmutov, V., Petäjä, T., Pieber, S. M., Praplan, A. P., Schobesberger, S., Steiner, G., Stozhkov,  
738 Y., Tomé, A., Tröstl, J., Wagner, A. C., Wagner, R., Williamson, C., Yan, C., Baltensperger, U.,  
739 Curtius, J., Donahue, N. M., Hansel, A., Kirkby, J., Kulmala, M., Worsnop, D. R., and Dommen, J.:  
740 Formation of highly oxygenated organic molecules from  $\alpha$ -pinene ozonolysis: chemical  
741 characteristics, mechanism, and kinetic model development, *ACS Earth Space Chem.*, 3, 873-883,  
742 <https://doi.org/10.1021/acsearthspacechem.9b00035>, 2019.

743 Nozière, B., Kalberer, M., Claeys, M., Allan, J., D'Anna, B., Decesari, S., Finessi, E., Glasius, M., Grgic,

744 I., and Hamilton, J. F.: The molecular identification of organic compounds in the atmosphere: state  
745 of the art and challenges, *Chem. Rev.*, 115, 3919-3983, 2015.

746 Orlando, J. J. and Tyndall, G. S.: Laboratory studies of organic peroxy radical chemistry: an overview  
747 with emphasis on recent issues of atmospheric significance, *Chem. Soc. Rev.*, 41, 6294-6317,  
748 <https://doi.org/10.1039/C2CS35166H>, 2012.

749 Otkjær, R. V., Jakobsen, H. H., Tram, C. M., and Kjaergaard, H. G.: Calculated hydrogen shift rate  
750 constants in substituted alkyl peroxy radicals, *J. Phys. Chem. A*, 122, 8665-8673,  
751 <https://doi.org/10.1021/acs.jpca.8b06223>, 2018.

752 Pye, H., Chan, A., Barkley, M., and Seinfeld, J.: Global modeling of organic aerosol: the importance of  
753 reactive nitrogen (NO<sub>x</sub> and NO<sub>3</sub>), *Atmos. Chem. Phys.*, 10, 11261-11276,  
754 <https://doi.org/10.5194/acp-10-11261-2010>, 2010.

755 Roger, Atkinson, Sara, M., Aschmann, James, N., Pitts, and Jr.: Rate constants for the gas-phase reactions  
756 of the OH radical with a series of monoterpenes at 294 ± 1 K, *Int. J. Chem. Kinet.*, 2004.

757 Shen, H., Vereecken, L., Kang, S., Pullinen, I., Fuchs, H., Zhao, D., and Mentel, T. F.: Unexpected  
758 significance of a minor reaction pathway in daytime formation of biogenic highly oxygenated  
759 organic compounds, *Sci. Adv.*, 8, eabp8702, <https://doi.org/10.1126/sciadv.abp8702>, 2022.

760 Sindelarova, K., Granier, C., Bouarar, I., Guenther, A., Tilmes, S., Stavrakou, T., Müller, J.-F., Kuhn, U.,  
761 Stefani, P., and Knorr, W.: Global data set of biogenic VOC emissions calculated by the MEGAN  
762 model over the last 30 years, *Atmos. Chem. Phys.*, 14, 9317-9341, [https://doi.org/10.5194/acp-14-](https://doi.org/10.5194/acp-14-9317-2014)  
763 [9317-2014](https://doi.org/10.5194/acp-14-9317-2014), 2014.

764 Tyndall, G., Cox, R., Granier, C., Lesclaux, R., Moortgat, G., Pilling, M., Ravishankara, A., and  
765 Wallington, T.: Atmospheric chemistry of small organic peroxy radicals, *J. Geophys. Res.-Atmos.*,  
766 106, 12157-12182, 2001.

767 Villenave, E. and Lesclaux, R.: Kinetics of the cross reactions of CH<sub>3</sub>O<sub>2</sub> and C<sub>2</sub>H<sub>5</sub>O<sub>2</sub> radicals with  
768 selected peroxy radicals, *J. Phys. Chem. C*, 100, 14372-14382, <https://doi.org/10.1021/jp960765m>,  
769 1996.

770 Wang, Y., Zhao, Y., Li, Z., Li, C., Yan, N., and Xiao, H.: Importance of hydroxyl radical chemistry in  
771 isoprene suppression of particle formation from  $\alpha$ -pinene ozonolysis, *ACS Earth Space Chem.*, 5,  
772 487-499, <https://doi.org/10.1021/acsearthspacechem.0c00294>, 2021.

773 Wolfe, G. M., Marvin, M. R., Roberts, S. J., Travis, K. R., and Liao, J.: The framework for 0-D  
774 atmospheric modeling (F0AM) v3. 1, *Geosci. Model Dev.*, 9, 3309-3319,  
775 <https://doi.org/10.5194/gmd-9-3309-2016>, 2016.

776 Xu, L., Møller, K. H., Crouse, J. D., Otkjær, R. V., Kjaergaard, H. G., and Wennberg, P. O.:  
777 Unimolecular reactions of peroxy radicals formed in the oxidation of  $\alpha$ -pinene and  $\beta$ -pinene by  
778 hydroxyl radicals, *J. Phys. Chem. A*, 123, 1661-1674, <https://doi.org/10.1021/acs.jpca.8b11726>,  
779 2019.

780 Yao, M., Zhao, Y., Hu, M., Huang, D., and Yan, N.: Multiphase reactions between secondary organic  
781 aerosol and sulfur dioxide: kinetics and contributions to sulfate formation and aerosol aging,  
782 *Environ. Sci. Technol. Lett.*, <https://doi.org/10.1021/acs.estlett.9b00657>, 2019.

783 Zhang, H., Yee, L. D., Lee, B. H., Curtis, M. P., Worton, D. R., Isaacman-VanWertz, G., Offenberg, J. H.,  
784 Lewandowski, M., Kleindienst, T. E., and Beaver, M. R.: Monoterpenes are the largest source of  
785 summertime organic aerosol in the southeastern United States, *Proc. Natl. Acad. Sci. U. S. A.*, 115,  
786 2038-2043, <https://doi.org/10.1073/pnas.1717513115>, 2018.

787 Zhao, Y., Thornton, J. A., and Pye, H. O. T.: Quantitative constraints on autoxidation and dimer formation

788 from direct probing of monoterpene-derived peroxy radical chemistry, Proc. Natl. Acad. Sci. U. S.  
789 A. , 115, 12142-12147, <https://doi.org/10.1073/pnas.1812147115>, 2018.

790 Zhao, Y., Yao, M., Wang, Y. Q., Li, Z. Y., Wang, S. Y., Li, C. X., and Xiao, H. Y.: Acylperoxy Radicals  
791 as Key Intermediates in the Formation of Dimeric Compounds in alpha-Pinene Secondary Organic  
792 Aerosol, Environ. Sci. Technol., 56, 14249-14261, 10.1021/acs.est.2c02090, 2022.

793 Zhao, Z. X., Zhang, W., Alexander, T., Zhang, X., Martin, D. B. C., and Zhang, H. F.: Isolating a-Pinene  
794 Ozonolysis Pathways Reveals New Insights into Peroxy Radical Chemistry and Secondary Organic  
795 Aerosol Formation, Environ. Sci. Technol., 55, 6700-6709, 10.1021/acs.est.1c02107, 2021.

796